UCRL-JRNL-232184

LAWRENCE
LIVERMORE
NATIONAL
LABORATORY

# The Gemini Deep Planet Survey - GDPS

D. Lafreniere, R. Doyon, C. Marois, D. Nadeau, B. R. Oppenheimer, P. F. Roche, F. Rigaut, J. R. Graham , R. Jayawardhana, D. Johnstone, P. G. Kalas, B. Macintosh, R. Racine

June 27, 2007

The Astrophysical Journal

**Disclaimer**

This document was prepared as an account of work sponsored by an agency of the United States Government. Neither the United States Government nor the University of California nor any of their employees, makes any warranty, express or implied, or assumes any legal liability or responsibility for the accuracy, completeness, or usefulness of any information, apparatus, product, or process disclosed, or represents that its use would not infringe privately owned rights. Reference herein to any specific commercial product, process, or service by trade name, trademark, manufacturer, or otherwise, does not necessarily constitute or imply its endorsement, recommendation, or favoring by the United States Government or the University of California. The views and opinions of authors expressed herein do not necessarily state or reflect those of the United States Government or the University of California, and shall not be used for advertising or product endorsement purposes.

# The Gemini Deep Planet Survey – GDPS[1]

David Lafrenière[a], René Doyon[a], Christian Marois[b], Daniel Nadeau[a], Ben R. Oppenheimer[c], Patrick F. Roche[d], François Rigaut[e], James R. Graham[f], Ray Jayawardhana[g], Doug Johnstone[h], Paul G. Kalas[f], Bruce Macintosh[b], René Racine[a]

david@astro.umontreal.ca doyon@astro.umontreal.ca cmarois@igpp.ucllnl.org
nadeau@astro.umontreal.ca bro@amnh.org pfr@astro.ox.ac.uk frigaut@gemini.edu
jrg@astron.berkeley.edu rayjay@astro.utoronto.ca
doug.johnstone@cnrc-nrc.hia.ca kalas@astron.berkeley.edu
bmac@igpp.ucllnl.org racine@astro.umontreal.ca

## ABSTRACT

We present the results of the Gemini Deep Planet Survey, a near-infrared adaptive optics search for giant planets and brown dwarfs around nearby young stars. The observations were obtained with the Altair adaptive optics system at the Gemini North telescope and angular differential imaging was used to suppress the speckle noise of the central star. Detection limits for the 85 stars observed are presented, along with a list of all faint point sources detected around them. Typically, the observations are sensitive to angular separations beyond 0.5″ with $5\sigma$ contrast sensitivities in magnitude difference at 1.6 $\mu$m of 9.6 at 0.5″, 12.9

[a]Département de physique and Observatoire du Mont Mégantic, Université de Montréal, C.P. 6128 Succ. Centre-Ville, Montréal, QC, H3C 3J7, Canada

[b]Institute of Geophysics and Planetary Physics L-413, Lawrence Livermore National Laboratory, 7000 East Ave, Livermore, CA 94550

[c]Department of Astrophysics, American Museum of Natural History, Central Park West at 79th Street, New York, NY 10024

[d]Astrophysics, Physics Department, University of Oxford, 1 Keble Road, Oxford, OX1 3RH, UK

[e]Gemini Observatory, Southern Operations Center, Association of Universities for Research in Astronomy, Inc., Casilla 603, La Serena, Chile

[f]Department of Astronomy, University of California at Berkeley, 601 Campbell Hall, Berkeley, CA 94720

[g]Department of Astronomy and Astrophysics, University of Toronto, 50 St. George Street, Toronto, ON, M5S 3H4, Canada

[h]National Research Council Canada, Herzberg Institute of Astrophysics, 5071 West Saanich Road, Victoria, BC, V9E 2E7, Canada

at 1″, 15 at 2″, and 16.6 at 5″. For the typical target of the survey, a 100 Myr old K0 star located 22 pc from the Sun, the observations are sensitive enough to detect planets more massive than 2 $M_{\rm Jup}$ with a projected separation in the range 40–200 AU. Depending on the age, spectral type, and distance of the target stars, the minimum mass that could be detected with our observations can be ∼1 $M_{\rm Jup}$. Second epoch observations of 48 stars with candidates (out of 54) have confirmed that all candidates are unrelated background stars. A detailed statistical analysis of the survey results, which provide upper limits on the fractions of stars with giant planet or low mass brown dwarf companions, is presented. Assuming a planet mass distribution $\mathrm{d}n/\mathrm{d}m \propto m^{-1.2}$ and a semi-major axis distribution $\mathrm{d}n/\mathrm{d}a \propto a^{-1}$, the upper limits on the fraction of stars with at least one planet of mass 0.5–13 $M_{\rm Jup}$ are 0.29 for the range 10–25 AU, 0.13 for 25–50 AU, and 0.09 for 50–250 AU, with a 95% confidence level; this result is weakly dependent on the semi-major axis distribution power-law index. Without making any assumption on the mass and semi-major axis distributions, the fraction of stars with at least one brown dwarf companion having a semi-major axis in the range 25–200 AU is $0.018^{+0.078}_{-0.014}$, with a 95% confidence level. The observations made as part of this survey have resolved the stars HD 14802, HD 135363, HD 160934, HD 166181, and HD 213845 into close binaries for the first time.

*Subject headings:* Planetary systems — stars: imaging — binaries: close — stars: low-mass, brown dwarfs

## 1. Introduction

More than 200 exoplanets have been discovered over the last decade through precise measurements of variations of the radial velocity (RV) of their primary star. Besides establishing that at least 6–7% of FGK stars have at least one giant planet with a semi-major axis smaller than 5 AU (Marcy et al. 2005), the profusion of data following from the RV discoveries has propelled the field of giant planet formation and evolution into an unprecedented state of activity. For a review of the main characteristics of the RV exoplanets, the

[1]Based on observations obtained at the Gemini Observatory, which is operated by the Association of Universities for Research in Astronomy, Inc., under a cooperative agreement with the NSF on behalf of the Gemini partnership: the National Science Foundation (United States), the Particle Physics and Astronomy Research Council (United Kingdom), the National Research Council (Canada), CONICYT (Chile), the Australian Research Council (Australia), CNPq (Brazil) and CONICET (Argentina).

reader is referred to Udry et al. (2007); Butler et al. (2006); Marcy et al. (2005). Besides the RV technique, the photometric transit method has lead successfully to the discovery of new exoplanets on small orbits (e.g. Konacki et al. 2003; Alonso et al. 2004; Cameron et al. 2007) and has provided the first measurements of the radius and mean density of giant exoplanets (e.g. Charbonneau et al. 2000). Very recently, a few exoplanets have been detected by gravitational microlensing (Bond et al. 2004; Udalski et al. 2005; Beaulieu et al. 2006; Gould et al. 2006); these planets have separations of ∼2–5 AU. Notwithstanding their great success in finding planets on small orbits, these techniques cannot be used to search for and characterize planets on orbits larger than ∼10 AU. As a result, the population of exoplanets on large orbits is currently unconstrained.

The two main models of giant planet formation are core accretion (Pollack et al. 1996) and gravitational instability (Boss 1997, 2001). In the core accretion model, solid particles within a proto-planetary disk collide and grow into solid cores which, if they become massive enough before the gas disk dissipates, trigger runaway gas accretion and become giant planets. Models predict that the timescale for formation of a planet like Jupiter through this process is about 5 Myr (Pollack et al. 1996), or about 1 Myr if migration of the core through the disk is allowed as the planet forms (Alibert et al. 2005). These timescales are comparable to or below the estimated proto-planetary dust disk lifetime (∼6 Myr, Haisch et al. 2001) and gas disk lifetime (several–10 Myr, Jayawardhana et al. 2006). Formation through core accretion is strongly dependent on the surface density of solid material in the proto-planetary disk (Pollack et al. 1996), precluding formation of Jupiter mass planets at distances greater than 15–20 AU, where the low density of planetesimals would lead to prohibitively long formation timescales. Neptune mass planets can be formed out to slightly larger distances.

In the gravitational instability model, small instabilities in a proto-planetary disk grow rapidly into regions of higher density that subsequently evolve into spiral arms owing to Keplerian rotation. Further interactions between these spiral arms lead to the formation of hot spots which then collapse to form giant planets. The range of orbital separation over which this mechanism may operate efficiently is not yet clear. Some studies indicate that it may lead to planet formation only at separations exceeding ∼100 AU (Whitworth & Stamatellos 2006; Matzner & Levin 2005), where the radiative cooling timescale is sufficiently short compared to the dynamical timescale, while others have been able to produce planets only at separations below 20–30 AU (Boss 2000, 2003, 2006).

A few other models are capable of forming giant planets on large orbits directly. One such mechanism is shock-induced formation following collision between disks (Shen & Wadsley 2006). In this model, the violent collision of two proto-planetary disks triggers instabilities

that lead to the collapse of planetary or brown dwarf (BD) mass clumps. Results of numerical simulations indicate that planets and BDs may form at separations of several tens of AU or more through this process (Shen & Wadsley 2006). The competitive accretion and ejection mechanism that was proposed initially to explain the formation of BD (Reipurth & Clarke 2001) could also form planetary mass companions on large orbits, as suggested by the results of recent simulations by Bate & Bonnell (2005).

Even in a scenario in which all giant planets form on small orbits, through either core accretion or gravitational collapse, a significant fraction of planets could be found on stable orbits of tens of AU because of outward orbital migration. Indeed, numerical simulations have shown that gravitational interactions between planets in a multi-planet system may send one of the planets, usually the least massive one, out to an eccentric orbit of semi-major axis of tens to hundreds of AU (Chatterjee et al. 2007; Veras & Armitage 2004; Rasio & Ford 1996; Weidenschilling & Marzari 1996). This process could be involved frequently in the shaping of the orbital parameters of planetary systems as we have learned from RV surveys that multi-planet systems are common, representing $\sim$14% of known planetary systems (Marcy et al. 2005). Outward migration of massive planets can be induced also by interactions between the planet and the gaseous disk; the simulations of Veras & Armitage (2004) reveal that this process is capable of carrying Jupiter mass planets out to several tens of AU. Similarly, angular momentum exchange between two planets (or more), achieved through viscous interactions with the disk, could drive the outer planet to a separation of hundreds of AU (Martin et al. 2007). Outward planet migration can result further from interaction of the planet with the solid particles in the disk after the gas has dissipated (e.g. Levison et al. 2007); there is in fact strong evidence that this mechanism has played an important role in the Solar system (Fernandez & Ip 1984; Malhotra 1995; Hahn & Malhotra 2005). Based on numerical simulations, it is likely that all giant planets of the Solar system formed interior to $\sim$15 AU and migrated outward (except Jupiter) to their current location (Tsiganis et al. 2005).

From an observational point of view, there is some evidence that planets on large orbits may exist. Many observations of dusty disks around young stars, made either in emitted light (e.g. Vega, $\varepsilon$ Eri, Fomalhaut; Holland et al. 1998; Greaves et al. 1998) or in scattered light (e.g. HD 141569, HR 4796, Fomalhaut; Augereau et al. 1999; Weinberger et al. 1999; Schneider et al. 1999; Kalas et al. 2005), have unveiled asymmetric or ring-like dust distributions. These peculiar morphologies could arise from gravitational dust confinement imposed by one or more (unseen) giant planets on orbits of tens to hundreds of AU. In fact, detailed numerical simulations of the effect of giant planets on the dynamical evolution of dusty disks have been able to reproduce the observed morphologies with remarkable agreement (Ozernoy et al. 2000; Wilner et al. 2002; Deller & Maddison 2005). Typically, Jupiter mass planets on

orbits of ∼60 AU are needed to reproduce the observations.

In the last few years, there have been a few discoveries of planetary mass or low-mass BD companions located beyond several tens of AU from their primary: an ∼8 $M_{\rm Jup}$ companion 40 AU from the BD 2M 1207−3932 (Mohanty et al. 2007; Chauvin et al. 2005a, 2004), a ∼25 $M_{\rm Jup}$ companion 100 AU from the T Tauri star GQ Lup (Marois et al. 2007; Seifahrt et al. 2007; Neuhäuser et al. 2005), a ∼12 $M_{\rm Jup}$ companion 210 AU from the young star CHXR 73 (Luhman et al. 2006), a ∼25 $M_{\rm Jup}$ companion 240 AU from the young BD 2M 1101−7732 (Luhman 2004), a ∼12 $M_{\rm Jup}$ companion 260 AU from the young star AB Pic (Mohanty et al. 2007; Chauvin et al. 2005b), a 7–19 $M_{\rm Jup}$ companion 240–300 AU from the young BD Oph 1622−2405 (Luhman et al. 2007a; Close et al. 2007; Jayawardhana et al. 2006), an ∼11 $M_{\rm Jup}$ companion 330 AU from the T Tauri star DH Tau (Luhman et al. 2006; Itoh et al. 2005), and a ∼21 $M_{\rm Jup}$ companion 790 AU from the star HN Peg (Luhman et al. 2007b). These discoveries might indicate that more similar companions, and less massive ones, do exist and remain to be found.

Perhaps even more compelling is the fact that the number of exoplanets found by RV surveys increases as a function of semi-major axis for the range 0.1–3 AU (Butler et al. 2006); these surveys are incomplete at larger separations. Conservative extrapolation suggests that there may be at least as many planets with semi-major axis beyond 3 AU as there are below (Butler et al. 2006). In fact, long-term trends in RV data have been detected for about 5% of the stars surveyed (Marcy et al. 2005), suggesting the presence of planets between 5 AU and 20 AU around them.

Given all of the considerations above, it is clear that a determination of the frequency of giant planets as a function of orbital separation out to hundreds of AU is necessary to elucidate the relative importance of the various modes of planet formation and migration. Direct imaging is currently the only viable technique to probe for planets on large separations and achieve this goal. However, detecting giant planets directly through imaging is very difficult due to the angular proximity of the star and the very large luminosity ratios involved. Currently, the main technical difficulty when trying to images giant planets directly does not come from diffraction of light by the telescope aperture, from light scattering due to residual atmospheric wavefront errors after adaptive optics (AO) correction, nor from photon noise of the stellar point spread function (PSF), but rather from light scattering by optical imperfections of the telescope and camera which produce bright quasi-static speckles in the PSF of the central star. These speckles are usually much brighter than the planets sought after. More in depth discussions of this problem, as well as possible venues to circumvent it using current instrumentation, can be found in Lafrenière et al. (2007); Hinkley et al. (2007); Marois et al. (2006, 2005); Masciadri et al. (2005); Biller et al. (2004); Schneider &

Silverstone (2003); Marois et al. (2003); Sparks & Ford (2002); Marois et al. (2000); Racine et al. (1999).

Many direct imaging searches for planetary or brown dwarf companions to stars have been done during the last five years, see for example Biller et al. (2007); Chauvin et al. (2006); Lowrance et al. (2005); Masciadri et al. (2005); McCarthy & Zuckerman (2004); Luhman & Jayawardhana (2002). Depending on the observing strategy employed, the properties of the target stars, and the characteristics of the instrument used, each of these surveys was sensitive to a different regime of companion masses and separations. Typically, these surveys have reached detection contrasts of 10–13 mag for angular separations beyond $1''$–$2''$, sufficient to detect planets more massive than $\sim$5 $M_{\rm Jup}$ for targets aged $\sim$100 Myr. Unfortunately, rigorous statistical analyses allowing derivation of clear constraints on the population of planets in the regimes of mass and separation to which these surveys were sensitive are currently not available in the literature; an assessment of the current status of knowledge is thus rather difficult to make. Nonetheless, it is fair to say that the population of planets less massive than $\sim$5 $M_{\rm Jup}$, having orbits with a semi-major axis of tens to hundreds of AU, is poorly constrained. Further, the question of the existence of a brown dwarf desert around stars at separations of a few tens to a few hundreds of AU has not been settled yet.

In this paper we report the results of the Gemini Deep Planet Survey (GDPS), a direct imaging survey of 85 nearby young stars aimed at constraining the population of Jupiter mass planets with orbits of semi-major axis in the range 10-300 AU. The selection of the GDPS target sample is explained in §2, and the observations and data reduction are detailed in §3. The detection limits achieved for each target are then presented in §4 along with all candidate companions detected. Statistical analyses of the results allowing determination of the maximum fraction of stars that could bear planetary companions are presented in §5. Concluding remarks follow in §6.

## 2. Target sample

In light of the luminosity ratio and angular separation problem highlighted above, the list of target stars was assembled mainly on the basis of young age and proximity to the Sun, the latter yielding a larger angular separation for a given physical distance between the star and an eventual planet. Equivalently, a given detection threshold is achieved at a smaller physical separation for a star closer to the Sun, and planets on smaller orbits can be detected. Additionally, for angular separations where planet detection is limited by sky background noise or read noise, planets of lower masses can be detected around a star closer to the Sun as their apparent brightness would be larger. Giant planets are intrinsically more luminous

at young ages and fade with time (e.g. Marley et al. 2007; Baraffe et al. 2003; Burrows et al. 1997); therefore, for a given detection threshold, observations of younger stars are sensitive to planets having a lower mass. The proximity and age criteria used in building the target list thus maximize the range of mass and separation over which the survey is sensitive.

The target stars were selected from three sources: (1) Tables 3 and 4 of Wichmann et al. (2003), which list nearby stars with an estimated age below or comparable to that of the Pleiades (∼100 Myr), based on measurements of lithium abundance, space velocity, and X-ray activity; (2) Tables 2 and 5 of Zuckerman & Song (2004b), which list members of the $\beta$ Pictoris (∼12 Myr) and AB Doradus (∼50 Myr) moving groups respectively; and (3) Tables 2 and 5 of Montes et al. (2001b), which list late-type single stars that are possible members of the Local Association (Pleiades moving group, 20–150 Myr) and IC 2391 supercluster (35–55 Myr) respectively, based on space velocity measurements. The stars listed in Montes et al. (2001b) were initially selected based on various criteria indicative of youth, such as kinematic properties, rotation rate, chromospheric activity, lithium abundance, or X-ray emission, but for many of these stars the space velocity is the only indication of youth as other measurements are either unavailable or inconclusive; the young age of such stars is therefore uncertain. This uncertainty will be taken into account in our statistical analysis (§5). A few stars known to have a circumstellar disk were added to these lists.

From this preliminary compilation, we have retained only stars with a distance smaller than 35 pc, and we have excluded stars of declination below $-32°$ since observations were to be made from the Gemini North observatory. Finally, we have further excluded stars indicated to be multiple in Zuckerman & Song (2004b). This procedure yielded a list of slightly over 100 target stars, of which 85 were actually observed. The properties of these 85 stars are presented in Table 1 and Figure 1. The median spectral type of our sample is K0, the median $H$ magnitude is 5.75, the median distance is 22 pc, the median proper motion amplitude is 240 mas yr$^{-1}$, and the median [Fe/H] is 0.00 dex (standard deviation of 0.21 dex).

Despite our effort to select only single stars, our observations show that 16 of the 85 target stars are close double or triple systems; this is indicated in the last column of Table 1. A thorough review of the literature revealed that 11 of these were known at the time the target list was compiled, three of which are astrometric binaries that had never been resolved prior to our observations (HD 14802, HD 135363, and HD 166181). Three other multiple systems were resolved with AO only after the target list was compiled (HD 77407, HD 129333, and HD 220140). Finally, the stars HD 160934 and HD 213845 are reported as binaries for the first time here. The five newly resolved binary systems are discussed further in §4.3.

Age estimates for the stars in our sample, needed to convert the observed contrasts

into mass detection limits using evolution models of giant planets,[2] are reported in Table 1 along with the references used for their determination. Whenever possible, we have used ages stated explicitly in the literature or the age of the association to which a star belongs. When no specific age estimate was available for stars taken from Wichmann et al. (2003), ages of 10–50 Myr or 50–150 Myr were assigned to the stars having a lithium abundance above or comparable to that of the Pleiades, respectively. For other stars that have lithium and/or X-ray measurements, ages were estimated from a comparison of the Li I 6708 Å equivalent width and/or the ratio of the X-ray to bolometric luminosity with Figures 3 and/or 4 of Zuckerman & Song (2004b) respectively. When lithium or X-ray measurements were not available, the kinematic ages were used as lower limits while the ages derived from the chromospheric activity index, $\log R_{\rm HK}$, were used as upper limits, as Song et al. (2004) showed that the latter ages tend to be systematically higher than those derived from lithium abundance or X-ray emission. When only the value of $\log R_{\rm HK}$ was available, the calibration of Donahue (1993)[3] was used to obtain an age estimate. Finally, when only kinematics measurements were available for a given star, an age of 100–5000 Myr or 50–5000 Myr was assigned if the star is a possible member of the Local Association or the IC 2391 supercluster respectively.

## 3. Observations and image processing

### 3.1. Data acquisition and observing strategy

All observations were obtained at the Gemini North telescope with the Altair adaptive optics system (Herriot et al. 2000) and the NIRI camera (Hodapp et al. 2003) (programs GN-2004B-Q-14, GN-2005A-Q-16, GN-2005B-Q-4, GN-2006A-Q-5, and GN-2006B-Q-5). The $f/32$ camera was used, yielding $0.022''$ pixel$^{-1}$ and a field of view of $22'' \times 22''$. The field lens of Altair was not used for any observation as it was not available for any of the first epoch observations. The observations were obtained in the narrow band filter CH4-short (1.54–1.65 $\mu$m), for the following reason. According to evolution models (e.g. Baraffe et al. 2003), planetary mass objects older than 10-20 Myr should have an effective temperature below 1000 K. Because of the large amounts of methane and the increased collision induced absorption by $H_2$ in their atmosphere, the near-infrared $K$-band flux of such objects is largely suppressed. It is thus more efficient to search for giant planets in either the $J$ or the $H$ band; the latter was preferred in this study because higher Strehl ratios are achieved

[2]It is assumed that any planet and its primary star would be coeval.

[3]This calibration is given explicitly in Henry et al. (1996).

at longer wavelengths. As the bulk of the $H$-band flux of cool giant planets is emitted in a narrow band centered at $\sim$1.58 $\mu$m because of important absorption by methane beyond 1.6 $\mu$m, it is even more efficient to search for these planets using the CH4-short filter, which is well matched to the peak of the emission. Based on evolution models and synthetic spectra of giant planets (Baraffe et al. 2003), it is expected that the mean flux density of a planet in the NIRI CH4-short filter be between 1.5 and 2.5 times higher than in the broad band $H$ filter, depending on the specific age and mass of the planet. These factors are consistent with the factors 1.6-2.0 calculated from the observed spectra of T7–T8 brown dwarfs, which have $T_{\rm eff} \sim 800$ K.

The angular differential imaging (ADI, Marois et al. 2006) technique was used to suppress the PSF speckle noise and improve our sensitivity to faint companions. This technique consists of acquiring a sequence of many exposures of the target using an altitude/azimuth telescope with the instrument rotator turned off (at the Cassegrain focus) to keep the instrument and telescope optics aligned. This is a very stable configuration and ensures a high correlation of the sequence of PSF images. This setup also causes a rotation of the field of view (FOV) during the sequence. For each target image in such a sequence, it is possible to build a reference image from other target images in which any companion would be sufficiently displaced due to FOV rotation. After subtraction of the reference image, the residual images are rotated to align their FOV and co-added. Because of the rotation, the residual PSF speckle noise is averaged incoherently, ensuring an ever improving detection limit with increasing exposure time. It has been shown that, for ADI with Altair/NIRI, the subtraction of an optimized reference PSF image from a target image can suppress the PSF speckle noise by a factor of $\sim$12, and that a noise suppression factor of $\sim$100 is achieved for the combination of 90 such difference images (Lafrenière et al. 2007; Marois et al. 2006).

An individual exposure time of 30 seconds was chosen for all targets. This exposure time is long enough so that, at large separation, faint companion detection is limited by sky background noise rather than read noise, and short enough so that the radius below which an image is saturated typically does not exceed 0.5″. The nominal observing sequence consisted of 90 images, but oftentimes a few images had to be discarded due to brief periods of very bad seeing, lost of tracking, or the advent of clouds. Short unsaturated exposures were acquired before and after the main sequence of (saturated) images for photometric calibration and Strehl ratio estimation; these observations were acquired in sub-array mode ($256\times256$ or $512\times512$ pixels), for which the minimum exposure time is shorter. Typically, an unsaturated sequence consisted of five exposures each obtained at a different dither position. The unsaturated observations are missing for a few targets as they were either skipped in the execution of the program, or they turned out to be saturated despite using the shortest possible exposure time. Table 2 summarizes all observations.

### 3.2. Data reduction

For each sequence of short unsaturated exposures, a sky frame was constructed by taking the median of the images obtained at different dither positions; this sky frame was subtracted from each image. The images were then divided by a flat field image. The PSFs of a given unsaturated sequence were registered to a common center and the median of the image sequence was obtained. The center of the PSFs were determined by fitting a 2-dimensional Gaussian function. As an indication of the quality of an observing sequence, the Strehl ratio was calculated by comparing the peak pixel value of the observed PSF image with that of an appropriate theoretical PSF. The calculated Strehl ratio values are reported in Table 2; two values are indicated for a target when unsaturated data were obtained before *and* after the main saturated sequence. Strehl ratios were typically in the range 10–20%.

Images of the main saturated sequence were first divided by a flat field image. Bad and hot pixels, as determined from analysis of the flat field image and dark frame respectively, were replaced by the median value of neighboring pixels. Field distortion was corrected using an IDL procedure provided by the Gemini staff (C. Trujillo, private communication) and modified to use the IDL *interpolate* function with cubic interpolation. The plate scale and field of view orientation for each image were obtained from the FITS header keywords.

For each sequence of saturated images, the stellar PSF of the first image was registered to the image center by maximizing the cross-correlation of the PSF diffraction spikes with themselves in a 180-degree rotation of the image about its center. The stellar PSF of the subsequent images was registered to the image center by maximizing the cross-correlation of the PSF diffraction spikes with those in the first image. Prior to shifting, the $1024\times1024$ pixel images were padded with zeros to $1450 \times 1450$ pixel to ensure that no FOV would be lost. An azimuthally symmetric intensity profile was finally subtracted from each image to remove the smooth seeing halo.

Next, the stellar PSF speckles were removed from each image by subtracting an optimized reference PSF image obtained using the "locally optimized combination of images" (LOCI) algorithm detailed in Lafrenière et al. (2007). The heart of this algorithm consists in dividing the target image into subsections and obtaining, for each subsection independently, an optimized reference PSF image consisting of a linear combination of the other images of the sequence for which the rotation of the FOV would have displaced sufficiently an eventual companion. For each subsection, the coefficients of the linear combination are optimized such that its subtraction from the target image minimizes the noise. The subsections geometry and the algorithm parameters determined in Lafrenière et al. (2007) were used for all targets. The residual images were then rotated to align their FOV and their median was obtained. Figure 2 illustrates the PSF subtraction process.

### 3.3. Photometric calibration and uncertainty

As the stellar PSF peak is saturated for the main sequence of images, and since much image processing is done to subtract the stellar PSF from each image, special care must be taken to calibrate the photometry of the residual images and ensure that the contrast limits calculated are accurate.

When the PSF peak is saturated, relative photometry can be calibrated by scaling the stellar flux measured in the unsaturated images obtained before and/or after the saturated sequence according to the ratio of the exposure times of the saturated and unsaturated images. However, the accuracy of this calibration method is affected by the (unknown) variations in Strehl ratio, hence of the peak PSF flux, that may have occurred between the saturated and unsaturated observations. To mitigate this problem, the calibration approach we adopted relies on a sharp ghost artifact located $(+0.09'', -2.45'')$ from the PSF center in the ALTAIR/NIRI images. Since the intensity of this ghost artifact is proportional to the PSF intensity, it can be used to infer the peak flux of a saturated PSF. This was verified for all sequences for which both unsaturated and saturated data were available. First, the stellar flux was measured in the unsaturated images using a circular aperture of diameter equal to the FWHM of the PSF. When unsaturated data were acquired both before and after the saturated sequence, the mean of the two values was used. Then the flux of the ghost artifact in the same aperture was measured for each image of the saturated sequence. The median of these values, scaled according to the ratio of the exposure times of the saturated and unsaturated images, was then compared to the stellar flux, and the process was repeated for all sequences that include both saturated and unsaturated data. Similar values were found for all sequences; the mean ratio of the flux of the ghost over that of the PSF peak was found to be $6.1 \times 10^{-5}$, with a standard deviation of $0.6 \times 10^{-5}$. Comparisons of the flux of background stars bright enough to be visible in each individual image of a sequence with the flux of the ghost in the corresponding images also confirmed that the intensity of the ghost is indeed directly proportional to the intensity of off-axis sources.

The procedure used for calibrating the photometry was the following. The flux of the ghost was measured for each image of a sequence and the median of these values, divided by the ratio quoted above, was taken to represent the peak stellar PSF flux, $F_\star$. This calibration method should be more accurate than the one based solely on unsaturated data obtained before and/or after the saturated sequence because the median ghost flux is affected in the same way as the median of all residual images by the variations of Strehl ratio that may have occurred during the sequence of saturated images or between the saturated and unsaturated measurements. For this reason, this calibration was used even for the sequences for which unsaturated data were available.

Observations obtained with ALTAIR without the field lens suffer from important off-axis Strehl degradation because of anisoplanatism; this degradation must be taken into account when calculating contrast. Unfortunately, it is virtually impossible to quantify the specific degradation pertaining to our data as there are no bright reference off-axis point sources available for every sequence of images. Instead, we have used the average anisoplanetism Strehl ratio degradation formula indicated on the ALTAIR webpage[4], which is $f_{\rm aniso}(\theta) \equiv S(\theta)/S_0 = {\rm e}^{-(\theta/12.5)^2}$, where $S(\theta)$ is the Strehl ratio at angular separation $\theta$, expressed in arcseconds, and $S_0$ is the on-axis Strehl ratio. This factor was used to correct the noise and the flux of faint point sources measured in the residual images.

As explained in Lafrenière et al. (2007), while the subtraction of an optimized reference PSF obtained using the LOCI algorithm leads to better signal-to-noise (S/N) ratios, it removes partially the flux of the point sources sought after. This flux loss must be accounted for when calculating contrast. This is done by calculating the normalized residual intensity, $f_{\rm sub}$, of artificially implanted point sources after execution of the subtraction algorithm; the method used is described in §4.3 of Lafrenière et al. (2007). Then using flux measurements made in the residual image, the factor $f_{\rm sub}$ is used to infer the true flux a point source, i.e. that before execution of the subtraction algorithm.

Another effect that must be taken into account for ADI data is the azimuthal smearing of an off-axis point source that occurs as the field of view rotates during an integration; this causes a fraction of the source's flux to fall outside of the circular aperture used for photometric measurements. The amount of flux loss in the aperture was calculated for each sequence of images as follows. For a given angular separation and for each image of a sequence, a copy of the unsaturated PSF was smeared according to its displacement during an integration. When no unsaturated data were available, a 2D Gaussian of the appropriate FWHM was used in place of the unsaturated PSF. The median of these smeared PSFs was obtained and the flux in a circular aperture was measured. This flux was divided by the flux of the original PSF in the same aperture to obtain the smearing factor $f_{\rm sm}$, which is used to correct the flux or noise measured in the images.

Given all of these considerations, the contrast at angular separation $\theta$ was calculated as

$$C(\theta) = \frac{F(\theta)}{f_{\rm aniso}(\theta) f_{\rm sm}(\theta) f_{\rm sub}(\theta)} \times \frac{1}{F_\star}, \tag{1}$$

where $F(\theta)$ is either the noise or the flux of a point source in a circular aperture of diameter equal to one PSF FWHM, at angular separation $\theta$, in the residual image. Eq. (1) was used

[4]http://www.gemini.edu/sciops/instruments/altair/altairCommissioningPerformance.html

for all contrast calculations in the present work. Typical correction factors as a function of angular separation are shown in Figure 3.

An estimate of the photometric accuracy resulting from the entire process was obtained by calculating the mean absolute difference between the magnitudes calculated at two epochs for every faint background star that was observed twice (see §4.2); this mean absolute difference was taken to represent $\sqrt{2}$ times the photometric uncertainty. This photometric uncertainty was found to vary significantly with angular separation, indicating that it is dominated by the uncertainty on the anisoplanatism factor. The photometric uncertainty as a function of angular separation is reported in Table 3; it is typically 0.07–0.15 mag for separations below $10''$. For completeness, it is noted that a higher photometric uncertainty, by about 0.08 mag, results when the unsaturated data obtained before and/or after the main sequence of saturated images are used to determine $F_\star$, rather than the median flux of the ghost artifact, justifying our choice to use the calibration based on the flux of the ghost for all sequences.

## 4. Results

### 4.1. Detection limits

To calculate detection limits, the residual images were first convolved by a circular aperture of diameter equal to one PSF FWHM, which is typically $\sim 0.07''$. The noise as a function of angular separation from the image center, $F(\theta)$, was then determined as the standard deviation of the pixel values in an annulus of width equal to one PSF FWHM. As shown in Lafrenière et al. (2007), the noise in an ADI residual image closely follows a Gaussian distribution (see also Marois et al., in preparation); it is thus appropriate to use a $5\sigma$ detection threshold for our data. The detection limits achieved for all target stars, expressed in magnitude difference, are presented in Table 4. The last two lines of this table present the median and best contrast, over the 85 observations, achieved at each angular separation. The median detection limits in magnitude difference are 9.6 at $0.5''$, 12.9 at $1''$, 15 at $2''$, and 16.6 at $5''$. The detection limits are presented graphically in Figure 4 for targets representative of poor, median, and good contrast performance.

One must resort to evolution models of giant planets to convert the detection limits mentioned above into mass limits. Traditionally, such evolution models have assumed arbitrary initial conditions for the planets (e.g. Baraffe et al. 2003; Burrows et al. 1997), with the caution that their results depend on the specific initial conditions adopted for ages below a few million years (Baraffe et al. 2002). Recent evolution models (Marley et al. 2007) that

incorporate initial conditions calculated explicitly based on models of planet formation indicate that it may in fact take as much as 10–100 Myr before the planets "forget" their initial conditions. Nevertheless, at the typical ages of our target stars, 50–300 Myr, all evolution models should agree reasonably well and yield similar mass detection limit estimates. In this work, we have used the COND evolution models of Baraffe et al. (2003), for which absolute $H$-band magnitudes as a function of mass and age are readily available. The following procedure was used to estimate the contrast, in the NIRI CH4-short filter, of a planet of given mass orbiting a given target. The absolute $H$-band magnitude of the planet was first obtained directly from the evolution models of Baraffe et al. (2003) and converted into an apparent magnitude, $H_{\rm pl}$, using the distance of the star. The corresponding magnitude in the NIRI CH4-short filter was then calculated as

$$m_{\rm pl} = H_{\rm pl} - 2.5 \log \left( \frac{f_{\rm CH4}}{f_H} \right), \tag{2}$$

where $f_{\rm CH4}$ and $f_H$ are the mean flux density of the planet in the NIRI CH4-short and broad band $H$ filters, respectively; their values were calculated using a synthetic spectrum of appropriate effective temperature and surface gravity (Baraffe et al. 2003; Allard et al. 2001)[5]. The stellar magnitudes in the NIRI CH4-short and broad band $H$ filters were assumed to be equal, such that the contrast of the planet was obtained as $m_{\rm pl} - H_\star$, where $H_\star$ is the $H$-band apparent magnitude of the target star. The $5\sigma$ contrast levels of planets of various masses orbiting a K0 primary of 100 Myr,[6] the typical target of the survey, are presented in Figure 4. For a typical target located at 22 pc from the Sun, the median detection limits correspond to 10.7 $M_{\rm Jup}$ at 11 AU, 3.9 $M_{\rm Jup}$ at 22 AU, 1.9 $M_{\rm Jup}$ at 44 AU, and 1.3 $M_{\rm Jup}$ at 110 AU.

The typical contrast reached by our survey improves on earlier surveys (e.g. Lowrance et al. 2005; Masciadri et al. 2005; Chauvin et al. 2006; Biller et al. 2007) by at least 1 mag at 1″, 1.5 mag at 2″, and $\sim$ 3 mag at larger separations. At a separation of 0.5″, the detection limits of our survey are similar to those achieved with the SDI device at the Very Large Telescope (Biller et al. 2007). The contrast reached by GDPS observations is thus the highest that has been achieved to date at separations larger than 0.5″–1″.

[5]Spectra available at ftp://ftp.ens-lyon.fr/pub/users/CRAL/fallard/

[6]An $H$-band absolute magnitude of 4.0 was used, this is the mean value of the K0 stars in the sample.

### 4.2. Candidate companion detections

To identify candidate companions, the residual images were first convolved by a circular aperture of diameter equal to one PSF FWHM, and then converted to signal-to-noise (S/N) images that were visually inspected for point sources at a $\gtrsim 5\sigma$ level. After identification of a point source, its position was measured by fitting a 2D Gaussian function, and its flux was measured in an aperture of diameter equal to one PSF FWHM; both operations were done in the non-convolved residual image. The contrast of the point source was then calculated using Eq.(1). More than 300 faint point sources were found around 54 targets, 173 of which are found around only 5 stars located at low galactic latitudes. Up to now, all but six of the 54 stars with candidates were re-observed at a subsequent epoch to verify whether or not the faint point sources detected are co-moving with the target star.

All candidate exoplanets observed at two epochs have been confirmed to be background sources by comparing their displacement between the two epochs with the expected displacement of a distant background source, based on the proper motion and parallax of the target; an example of this verification is presented in Figure 5. As a reference for future planet searches, a compilation of all faint point sources identified around our target stars is presented in Table 5.

An estimate of the uncertainties on the measured separations and position angles (P.A.) was obtained by calculating the mean absolute difference between the separation and P.A. measured at the second epoch and those predicted for this epoch based on the parallax and proper motion of the target stars. Given the high precision on the parallax and proper motion of the target stars, the differences observed are dominated by our measurement uncertainties. The mean absolute differences calculated are taken to represent $\sqrt{2}$ times the uncertainties; values of $\sigma_{\rm sep} = 0.015''$ and $\sigma_{\rm P.A.} = 0.2^\circ$ are found.

### 4.3. Newly resolved binary systems

As mentioned in §2, 16 of the target stars are part of multiple systems. Four of these systems were resolved into binaries for the first time by our observations, and a fifth was found to be a relatively large separation binary system for which there was no prior indication in the literature. These five systems are discussed below, and a summary of their properties is given in Table 6.

**HD 14802** A source $12 \pm 2$ times fainter than HD 14802 was detected at a separation of $0.469'' \pm 0.005''$ and P.A. $267.1^\circ \pm 0.7^\circ$ (epoch 2005.6348); the flux ratio is uncertain

because the peak of the primary star PSF is saturated. Common proper motion of the pair was not verified but the system is likely bound given the brightness and close separation of the companion. The Hipparcos catalog (Perryman & ESA 1997) indicates that the proper motion of this star is accelerating and the star is likely part of a binary system; an astrometric solution for the system was obtained by Gontcharov et al. (2000). The estimated period and semi-major axis are 25 yr and 0.5″, respectively, consistent with the projected separation we have measured.

**HD 135363** This star was recognized as an astrometric binary by Wielen et al. (2000)[7], and later by Makarov & Kaplan (2005); no astrometric solution is available in the literature. We have detected a companion to HD 135363 at a separation of $0.302'' \pm 0.002''$ and P.A. of $129.9^\circ \pm 0.5^\circ$ (epoch 2005.2950); the companion is a factor $4.0 \pm 0.1$ fainter than the primary. Second epoch observations have confirmed that the pair is physically bound, see Figure 6. The projected separation of the system is ∼9 AU.

**HD 160934** This star has a known mid-M dwarf companion at a separation of 19″ and P.A. of 151° (Lowrance et al. 2005; Weis 1991). Very recently, HD 160934 was found to be a spectroscopic binary by Gálvez et al. (2006); they obtained a preliminary orbital solution with a period of 17.1 year, eccentricity 0.8, and secondary mass corresponding to an M2-M3V spectral type. Our observations have resolved HD 160934 into a tight binary. The companion is located at a separation of $0.213'' \pm 0.002''$ and P.A. of $268.5^\circ \pm 0.7^\circ$ (epoch 2005.2953) from the primary, and is fainter by a factor $2.2 \pm 0.1$. Observations at two epochs have confirmed that the pair is bound, see Figure 7. The projected separation of the tight pair is ∼5.2 AU. Given the 17-year orbital period mentioned above, and using a very crude estimate of the total mass ($m_{\rm tot} \sim 1.1$) based on the spectral types of the components, we estimate that the semi-major axis of the companion found by radial velocity is roughly 7 AU. Given the eccentricity of 0.8, the projected separation of this companion should be $< 12$ AU, consistent with the separation we have observed. The contrast of the pair we have resolved (0.86 mag) is also consistent with the companion being of early-M spectral type. Thus we believe that we have found the same companion as that found by radial velocity.

**HD 166181** This star has been known for a long time to be a spectroscopic binary with a period of only 1.8 days (Nadal et al. 1974). More recently, analysis of additional radial velocity data has lead Dempsey et al. (1996) to propose that the system is in fact triple; a

[7]see http://www.ari.uni-heidelberg.de/datenbanken/dmubin/dmubin.html

proposition which was confirmed by Fekel et al. (2005), who found radial velocity variations ascribable to a third component with an orbit of period 5.7 year and eccentricity 0.765. Further, by reanalyzing Hipparcos data in light of this new component, these authors have found a new astrometric solution for the system, leading to revised values of parallax and proper motion (see Table 1) and to a determination of the orbital inclination of the long-period companion. Based on their complete solution, they estimate the semi-major axis of the outer companion at 0.077″ (2.5 AU) and its mass at 0.79 $M_{\odot}$. Our observations have resolved the long-period companion of this triple system. In 2005.2926, the companion was located at a separation of $0.065'' \pm 0.005''$ and P.A. of $16.2° \pm 5.0°$, and in 2006.7124, it was located at a separation of $0.102'' \pm 0.003''$ and P.A. of $51.5° \pm 2.0°$. The evolution of the separation and P.A. of this source between the two epochs is far from that expected for an unrelated background source and is in very good agreement with the orbital motion expected based on the astrometric solution of Fekel et al. (2005) (see Fig. 8), confirming that the source observed is HD 166181B. The flux ratio of the component Aab to component B is ∼5.5, a contrast of ∼1.85 mag.

**HD 213845** A bright source is visible in our data at a separation of $6.09'' \pm 0.03''$ and P.A. of $129.8° \pm 0.4°$ from HD 213845 (epoch 2005.6453). This source did not change separation nor P.A. between our 2005 and 2006 observations (see Figure 9), indicating that it is bound to HD 213845. The companion is only visible in our saturated data as its separation exceeds the field of view of the sub-array used for the unsaturated observations. Further, being relatively bright, the peak of the companion's PSF is saturated in all our data, making it very difficult to estimate its flux ratio to the primary and explaining the larger uncertainty on the separation and P.A. quoted above. The companion was possibly detected by 2MASS, but its measured position and photometry in the 2MASS point source catalog (PSC) are affected by confusion due to the nearby primary. Nevertheless, the relative position of this source in the 2MASS PSC, separation of 5.55″ and P.A. of 128°, is consistent with the star being gravitationally bound to HD 213845 as, were it not a bound companion, its separation should have changed by ∼2″ between the 2MASS observations and our first epoch observations. Although the separation of this binary system is well above the resolution limit of seeing-limited observations, we have found no prior indication of binarity in the literature.

## 5. Analysis and discussion

The detection limits determined in §4.1 can be used to calculate an upper limit to the fraction of stars that have companions of mass and semi-major axis inside some given

intervals. The analysis presented in this section is largely guided by the work of Brandeker et al. (2006); Carson et al. (2006); Allen et al. (2005); and Sivia (1996). The statistical formalism for the analysis is presented first and various applications to our data are presented afterward.

### 5.1. Statistical formalism

Consider the observation of $N$ stars enumerated by $j = 1 \ldots N$. Let $f$ be the fraction of stars that have at least one companion of mass and semi-major axis in the intervals $[m_{\rm min}, m_{\rm max}]$ and $[a_{\rm min}, a_{\rm max}]$, respectively, and $p_j$ the probability that such a companion around star $j$, if indeed it was there, would be detected given the detection limits of the observations. The probability of detecting such a companion around star $j$ is $fp_j$, and the probability of not detecting a companion around this star is simply $1 - fp_j$. If the set $\{d_j\}$ denotes the detections made by the observations, such that $d_j$ equals 1 if a companion is detected around star $j$ or else equals 0, then the probability that the observed outcome would occur, also called the likelihood of the data given $f$, is given by

$$\mathcal{L}(\{d_j\}|f) = \prod_{j=1}^{N} (1 - fp_j)^{(1-d_j)} (fp_j)^{d_j} . \tag{3}$$

According to Bayes' theorem, from the *a priori* probability density $p(f)$, or prior distribution, and the likelihood function $\mathcal{L}$, one may calculate $p(f|\{d_j\})$, the probability density updated in light of the data, or posterior distribution:

$$p(f|\{d_j\}) = \frac{\mathcal{L}(\{d_j\}|f)p(f)}{\int_0^1 \mathcal{L}(\{d_j\}|f)p(f)\mathrm{d}f}. \tag{4}$$

In this study, since we have no prior knowledge about $f$, we use the most ignorant prior distribution $p(f) = 1$.

The posterior distribution $p(f|\{d_j\})$ can be used to determine a confidence interval (CI) for $f$, bounded by $f_{\rm min}$ and $f_{\rm max}$, for a given confidence level (CL) $\alpha$. For a case where there is no detection, as is the case with our survey, then clearly $f_{\rm min} = 0$, and the upper bound of the CI is found by solving

$$\alpha = \int_0^{f_{\rm max}} p(f|\{d_j\})\mathrm{d}f. \tag{5}$$

For a case where there are some detections, an equal-tail CI is found by solving

$$\frac{1-\alpha}{2} = \int_0^{f_{\rm min}} p(f|\{d_j\})\mathrm{d}f \quad \text{and} \quad \frac{1-\alpha}{2} = \int_{f_{\rm max}}^{1} p(f|\{d_j\})\mathrm{d}f. \tag{6}$$

In this work a value of $\alpha = 0.95$ was chosen.

The determination of the $p_j$'s is a critical step of this analysis; their value depends on the detection limits of the observations, on the ages and distances of the systems, and on the mass, semi-major axis, and orbital eccentricity distributions of the companions. In calculating the $p_j$'s it is also important to account properly for orbital inclination and phase as these affect significantly the distribution of projected separations for an orbit of given semi-major axis. In this work, the $p_j$'s were calculated using a Monte Carlo approach. The mass and semi-major axis intervals, $[m_{\rm min}, m_{\rm max}]$ and $[a_{\rm min}, a_{\rm max}]$, were first selected. Then for each target star, 10000 planets were generated by sampling randomly, for each planet, the mass, semi-major axis, orbital eccentricity, orbital separation projection factor, and age of the system. The mass and semi-major axis distributions are left arbitrary for the moment; different possibilities will be explored later. For all of our calculations, the orbital eccentricity distribution was assumed to be that of the radial velocity exoplanets sample, which is well fit by a Gaussian function of mean 0.25, standard deviation 0.19, and with $0 \leq e \leq 0.8$ (Marcy et al. 2005). The orbital separation projection factor was sampled using the method described in Appendix A of Brandeker et al. (2006); this method properly takes into consideration orbital eccentricities, phases, and orientations. The age was sampled uniformly within the range indicated in Table 1. Given the age assigned to each planet, the procedure described in 4.1 was used to convert its mass into a magnitude difference in the NIRI CH4-short filter. The projected physical separation of each planet was converted into an angular separation based on the distance of its primary star. Finally, given the sample of planets assigned to target $j$, the probability $p_j$ was calculated as the fraction of planets lying above the corresponding detection limits.

The above determination of the $p_j$'s yields a CI for $f$ that is a function of the assumptions made on the mass and semi-major axis distributions. For a case where there is no detection, it is also possible to obtain a more conservative estimate of $f_{\rm max}$ that is valid for any distributions of mass and semi-major axis. The procedure used to do this is identical to that described above except for the following. Rather than populating the whole intervals of mass and semi-major axis considered, all planets are assigned a mass and semi-major axis precisely equal to $m_{\rm min}$ and $a_{\rm min}$, respectively. Because more massive or more distant planets are easier to detect, the values of $p_j$'s calculated in this manner constitute lower limits to the values that would be obtained by populating the whole intervals assuming any specific distributions; accordingly, the resulting value of $f_{\rm max}$ constitutes an upper limit. This approach is perfectly legitimate as long as $a_{\rm max}$ is chosen such that the values of $p_j$'s for any $a$ in $[a_{\rm min}, a_{\rm max}]$ are at least as large as those for $a_{\rm min}$.

### 5.2. Model-independent upper limit on companion occurrence

As a first analysis of the survey results, we present model-independent estimates of $f_{\max}$ for $m_{\min}$ =1, 2, 3, 4, 5, 7.5, 10, and 13 $M_{\rm Jup}$, and for all $a_{\min}$ between 10 and 500 AU; these estimates were calculated according to the last procedure described above. For this analysis, and those in the next section, we have not considered the 6 stars with candidates for which second epoch observations are missing. The results obtained in this section are valid for any $m_{\max}$ up to $\sim$40 $M_{\rm Jup}$ as no companion with a mass below this value was detected.[8] The mean detection probability for a planet of given mass and semi-major axis, i.e. the average of the $p_j$'s over all $j$'s, is shown in Figure 10; this figure provides an indication of the sensitivity of our survey. The peak sensitivity of the survey occurs for semi-major axes between 50 and 200 AU; the peak values are $\sim$45% and $\sim$65% for 2 and 5 $M_{\rm Jup}$, respectively. The survey is particularly sensitive to brown dwarfs ($m \gtrsim 13$ $M_{\rm Jup}$), with a detection probability above 75% between 30 and 200 AU. A decline in sensitivity occurs at a separation of $\sim$200 AU; this is consistent with the field of view of the observations ($\sim$11″ radius) and mean distance of the targets (22 pc).

The results for $f_{\max}$ are shown in Figure 11. For a semi-major axis interval lower bound of 50 AU, the planet frequency upper limits are 0.29 for 1–13 $M_{\rm Jup}$ and 50–300 AU, 0.12 for 2–13 $M_{\rm Jup}$ and 50–300 AU, and 0.057 for 5–13 $M_{\rm Jup}$ and 50–180 AU. For a semi-major axis lower bound of 25 AU, the upper limits are 0.24 for 2–13 $M_{\rm Jup}$ and 25–440 AU and 0.09 for 5–13 $M_{\rm Jup}$ and 25–300 AU. For completeness, the exercise was repeated for circular orbits and for a uniform distribution of eccentricity (between 0 and 1), and the results obtained were very similar to those shown in Figure 11.

The results also indicate that no more than 0.052 of stars have low-mass brown dwarf companions ($13 < m/M_{\rm Jup} < 40$) between 25 and 240 AU. The brown dwarf companion to HD 130948 (Potter et al. 2002; Goto et al. 2002) must be taken into account explicitly for determining the frequency of stars with at least one companion in the whole brown dwarf mass range ($13 < m/M_{\rm Jup} < 75$). This analysis must be carried out with care as the semi-major axis of this companion could be significantly different from its measured projected physical separation of 47 AU. It is possible to account for this uncertainty by calculating the probability distribution of the real semi-major axis of the brown dwarf companion using a Monte Carlo approach similar to the one presented above for the calculation of the $p_j$'s. Basically, the projected separation of the companion is fixed at $s = 47$ AU and its orbital eccentricity and orbital projection factor are sampled randomly $10^5$ times, as described

[8]The previously known 40–65 $M_{\rm Jup}$ binary brown dwarf companion located 2.6″from HD 130948 (Potter et al. 2002; Goto et al. 2002) is detected in our data.

above. The de-projected semi-major axis is then calculated for each random trial and its normalized distribution over all trials is obtained. As the projection factor can never be larger than $(1 + e_{\rm max})$, where $e_{\rm max}$ is the maximum eccentricity allowed, the semi-major axis probability distribution is equal to zero below $s/(1 + e_{\rm max})$; the distribution extends to infinity for higher values. Applied to the current case, this calculation indicates that at a 95% CL the semi-major axis of the binary brown dwarf companion to HD 130948 lies in the interval 26–157 AU. We thus posit that our observations have resulted in one detection in the semi-major axis interval 25–200 AU and mass interval 13–75 $M_{\rm Jup}$; then using the procedure described in the previous section and Eq. (6), the frequency of stars with at least one brown dwarf companion in the semi-major axis interval 25–200 AU is $0.018^{+0.078}_{-0.014}$, with a 95% CL. This result is consistent with the upper limit of 0.12 (95% CL) reported by Carson et al. (2006) for the 25–100 AU semi-major axis interval.

### 5.3. Model-dependent upper limit on giant planet occurrence

In this section we derive first an upper limit to the fraction of stars harboring at least one planet in the single mass interval $[0.5, 13]$ $M_{\rm Jup}$, assuming that the mass distribution follows ${\rm d}n/{\rm d}m \propto m^{-1.2}$. The mass distribution adopted is based on a statistical analysis of the RV results that properly accounts for the detection sensitivity reached for each star (A. Cumming et al. 2007, in preparation) and is formally valid only for planets with semi-major axis below ∼3 AU; here it is blindly extrapolated to larger semi-major axes. For comparison, a simple fit of the mass distribution of the RV exoplanets sample yields ${\rm d}n/{\rm d}m \propto m^{-1.1}$ (Butler et al. 2006). For this calculation the whole mass interval is populated according to the distribution stated, but all planets are assigned a value $a_{\rm min}$ for the semi-major axis, so as to make the results independent of its distribution. The calculation was made for all $a_{\rm min}$ between 10 and 500 AU. The results are shown in Figure 12. At a 95% CL, the fraction of stars having at least one planet of mass in the range $[0.5, 13]$ $M_{\rm Jup}$ and semi-major axis in $[10, 500]$, $[25, 340]$, and $[50, 230]$ AU is less than 0.62, 0.17, and 0.10, respectively. For reference, results of the same analysis assuming ${\rm d}n/{\rm d}m \propto m^{\beta}$, with $\beta = 0$ and $-2$, are presented also in Figure 12. As expected, a smaller $\beta$ leads to larger values of $f_{\rm max}$ because a larger fraction of planets have a smaller mass, while a larger value of $\beta$ has the opposite effect.

Next we calculate upper limits for the same mass interval by assuming further that the distribution of semi-major axes follows ${\rm d}n/{\rm d}a \propto a^{\gamma}$, for $\gamma = -1$, 0, and 1. This range of power-law index includes the value of $\gamma = -0.67$ found by A. Cumming et al. (2007, in preparation) for the RV exoplanets sample within the range 0.03–3 AU. We have done the calculations for $a_{\rm min}$=10, 25, and 50 AU, and for all $a_{\rm max}$ in the range $[a_{\rm min} + 10, 500]$ AU;

the results are presented in Figure 13. At a 95% CL and for $\gamma = -1$, the upper limits to the fraction of stars with at least one planet of mass in the range $[0.5, 13]$ $M_{\rm Jup}$ are 0.29 for the semi-major axis range 10–25 AU, 0.19 for 10–50 AU, 0.13 for 25–50 AU, 0.11 for 25–100 AU, and 0.09 for 50–250 AU. Slightly smaller values of $f_{\rm max}$ are found for larger values of $\gamma$, as such indices would place more planets at larger separations where they would have been easier to detect with our observations. For the larger values of $a_{\rm min}$, the value of $\gamma$ has very little effect on the upper limit found as, no matter the value of $\gamma$, the majority of planets are located at separations for which the sensitivity of the observations is high. Overall, the weak dependence of $f_{\rm max}$ on $\gamma$ implies that the semi-major axis distribution cannot be constrained from our results.

## 6. Summary and conclusion

In this paper, we have presented the results of the Gemini Deep Planet Survey, which is a near-infrared adaptive optics search for giant planets on orbits of 10–300 AU around nearby young stars. The use of angular differential imaging at the Gemini North telescope has enabled us to reach the best sensitivities to date for detecting giant exoplanets with projected separations above $\sim$0.5″–1″. The typical detection limits reached by the survey, in magnitude difference between an off-axis point source and the central star, are 9.6 at 0.5″, 12.9 at 1″, 15 at 2″, and 16.6 at 5″, sufficient to detect planets more massive than 2 $M_{\rm Jup}$ with a projected separation of 45–200 AU around a typical target star. More than 300 faint point sources have been detected around 54 of the 85 stars observed, but observations at a second epoch have revealed changes in separation and P.A. of these point sources relative to the target stars that were all consistent with those expected from unrelated background objects. The observations made as part of this survey have resolved the stars HD 14802, HD 135363, HD 160934, HD 166181, and HD 213845 into close binaries for the first time.

We have presented a statistical analysis of the survey results to derive upper limits to the fraction of stars having planetary companions. This analysis indicates that, at a 95% CL, the fraction of stars harboring at least one planet more massive than 2 $M_{\rm Jup}$ with an orbit of semi-major axis in the range 25–440 AU or 50–300 AU is less than 0.24 or 0.12, respectively, independently of the mass and semi-major axis distributions of the planets; for planets more massive than 5 $M_{\rm Jup}$, the upper limits are 0.091 for 25-300 AU and 0.057 for 50–180 AU. It was also found that less than 0.052 of stars have low-mass brown dwarf companions ($13 < m/M_{\rm Jup} < 40$) between 25 and 240 AU (see Figure 11); this upper limit is set by the sample size only as the sensitivity of the observations to brown dwarfs is very good. Assuming a mass distribution following $\mathrm{d}n/\mathrm{d}m \propto m^{-1.2}$, the results indicate that, with a

95% CL, the fraction of stars having at least one planet of mass in the range 0.5–13 $M_{\rm Jup}$ and semi-major axis in the range 25–340 AU is less than 0.17, and less than 0.10 for the range 50–230 AU. Assuming further a semi-major axis distribution following $\mathrm{d}n/\mathrm{d}a \propto a^{-1}$, the upper limits to the fraction of stars with planets are 0.29 for the range 10–25 AU, 0.13 for 25–50 AU, and 0.09 for 50–250 AU.

The work presented in this paper constitutes a first step toward the detection of the population of "outer" giant planets around other stars. Such a study, which is complementary to RV searches in terms of orbital separation, is necessary to improve our understanding of the various mechanisms that could generate planets on orbits of tens to hundreds of AU, such as in situ formation triggered by collisions of stars with proto-planetary disks or orbital migration induced by gravitational scattering in multiple planet systems. While the results obtained in this survey provide evidence that the efficiency of these mechanisms is low, at least in the mass and semi-major axis ranges explored, the sample size and sensitivities reached are insufficient to tell if they operate at all, or which one is dominant. Future searches reaching better sensitivities and targeted at a larger sample of stars will be necessary to answer these questions.

Considerable efforts are currently deployed by major observatories to develop instruments dedicated to the search of giant exoplanets around nearby stars. The Gemini Planet Imager (GPI, Gemini Telescope, Macintosh et al. 2006a), the Spectro-Polarimetric High-contrast Exoplanet Research instrument (SPHERE, Very Large Telescope, Dohlen et al. 2006), and the Planet Formation Imager (PFI, Thirty-Meter Telescope, Macintosh et al. 2006b) are good examples; the first two should see their first light in around 2010, while PFI should begin operation in around 2015. These complex instruments will ally an extreme AO system to correct atmospheric wavefront errors to unprecedented levels of accuracy, a calibration system to correct instrumental quasi-static aberrations, a coronagraph to suppress the coherent on-axis stellar light, and differential imaging capabilities enabled by either multi-channel cameras or integral field spectrographs. The expected performance of these instruments, e.g. a contrast better than 17.5 mag at a separation of 0.5″ for GPI (Macintosh et al. 2006a), should allow detection of planets of 1 $M_{\rm Jup}$ aged less than 100–200 Myr at separations of 5–50 AU, significantly improving on the work presented here. These efforts should uncover the first instances of outer giant planets, if they exist, or place sufficient constraints on their existence to rule out the mechanisms that could generate them. In less than a decade the James Webb Space Telescope will allow similar studies to be done for relatively nearby M-type primaries, which are too faint for operating the wavefront sensor of extreme adaptive optics systems. Given all of the projects that should unfold in the next few years, the coming decade promises to be extremely exciting for exoplanet science.

The authors would like to thank the Gemini staff for carrying out all the observations. This project was made possible through the support and generous allocation of observing time from the Canadian, US, UK, and Gemini staff time allocation committees. This work was supported in part through grants from the Natural Sciences and Engineering Research Council, Canada, from the Fonds Québécois de la Recherche sur la Nature et les Technologies, and from the Faculté des Études Supérieures de l'Université de Montréal. This research was performed in part under the auspices of the US Department of Energy by the University of California, Lawrence Livermore National Laboratory under contract W-7405-ENG-48, and also supported in part by the National Science Foundation Science and Technology Center for Adaptive Optics, managed by the University of California at Santa Cruz under cooperative agreement AST 98-76783. This research has made use of the SIMBAD database, operated at Centre de Données astronomiques de Strasbourg (CDS), Strasbourg, France. This research has made use of the VizieR catalog service (Ochsenbein et al. 2000), hosted by the CDS.

## REFERENCES

Alibert, Y., Mordasini, C., Benz, W., & Winisdoerffer, C. 2005, A&A, 434, 343

Allard, F., Hauschildt, P. H., Alexander, D. R., Tamanai, A., & Schweitzer, A. 2001, ApJ, 556, 357

Allen, P. R., Koerner, D. W., Reid, I. N., & Trilling, D. E. 2005, ApJ, 625, 385

Alonso, R. et al. 2004, ApJ, 613, L153

Augereau, J. C., Lagrange, A. M., Mouillet, D., & Ménard, F. 1999, A&A, 350, L51

Baraffe, I., Chabrier, G., Allard, F., & Hauschildt, P. H. 2002, A&A, 382, 563

Baraffe, I., Chabrier, G., Barman, T. S., Allard, F., & Hauschildt, P. H. 2003, A&A, 402, 701

Barrado y Navascués, D., Stauffer, J. R., Song, I., & Caillault, J.-P. 1999, ApJ, 520, L123

Bate, M. R., & Bonnell, I. A. 2005, MNRAS, 356, 1201

Beaulieu, J.-P. et al. 2006, Nature, 439, 437

Biller, B. A., Close, L., Lenzen, R., Brandner, W., McCarthy, D. W., Nielsen, E., & Hartung, M. 2004, in Proc. SPIE, Vol. 5490, Advancements in Adaptive Optics, ed. D. Bonaccini Calia, B. L. Ellerbroek, & R. Ragazzoni, 389–397

Biller, B. A. et al. 2007, ArXiv e-prints, astro-ph/0705.0066

Bond, I. A. et al. 2004, ApJ, 606, L155

Boss, A. P. 1997, Science, 276, 1836

—. 2000, ApJ, 536, L101

—. 2001, ApJ, 563, 367

—. 2003, ApJ, 599, 577

—. 2006, ApJ, 637, L137

Brandeker, A., Jayawardhana, R., Khavari, P., Haisch, Jr., K. E., & Mardones, D. 2006, ApJ, 652, 1572

Burrows, A. et al. 1997, ApJ, 491, 856

Butler, R. P. et al. 2006, ApJ, 646, 505

Cameron, A. C. et al. 2007, MNRAS, 375, 951

Carpenter, J. M., Wolf, S., Schreyer, K., Launhardt, R., & Henning, T. 2005, AJ, 129, 1049

Carson, J. C., Eikenberry, S. S., Smith, J. J., & Cordes, J. M. 2006, AJ, 132, 1146

Cayrel de Strobel, G., Soubiran, C., Friel, E. D., Ralite, N., & Francois, P. 1997, A&AS, 124, 299

Cayrel de Strobel, G., Soubiran, C., & Ralite, N. 2001, A&A, 373, 159

Charbonneau, D., Brown, T. M., Latham, D. W., & Mayor, M. 2000, ApJ, 529, L45

Chatterjee, S., Ford, E. B., & Rasio, F. A. 2007, ArXiv Astrophysics e-prints, astro-ph/0703166

Chauvin, G., Lagrange, A.-M., Dumas, C., Zuckerman, B., Mouillet, D., Song, I., Beuzit, J.-L., & Lowrance, P. 2004, A&A, 425, L29

—. 2005a, A&A, 438, L25

Chauvin, G., Lagrange, A.-M., Udry, S., Fusco, T., Galland, F., Naef, D., Beuzit, J.-L., & Mayor, M. 2006, A&A, 456, 1165

Chauvin, G. et al. 2005b, A&A, 438, L29

Clem, J. L., VandenBerg, D. A., Grundahl, F., & Bell, R. A. 2004, AJ, 127, 1227

Close, L. M. et al. 2007, ApJ, 660, 1492

Deller, A. T., & Maddison, S. T. 2005, ApJ, 625, 398

Dempsey, R. C., Neff, J. E., O'Neal, D., & Olah, K. 1996, AJ, 111, 1356

Dohlen, K. et al. 2006, in Proc. SPIE, Vol. 6269, Ground-based and Airborne Instrumentation for Astronomy, ed. I. S. McLean & M. Iye, 62690Q

Donahue, R. A. 1993, PhD thesis, AA(New Mexico State Univ., University Park.)

Favata, F., Barbera, M., Micela, G., & Sciortino, S. 1995, A&A, 295, 147

Favata, F., Micela, G., Sciortino, S., & D'Antona, F. 1998, A&A, 335, 218

Fekel, F. C., Barlow, D. J., Scarfe, C. D., Jancart, S., & Pourbaix, D. 2005, AJ, 129, 1001

Fernandez, J. A., & Ip, W.-H. 1984, Icarus, 58, 109

Fuhrmann, K. 2004, Astronomische Nachrichten, 325, 3

Gaidos, E. J. 1998, PASP, 110, 1259

Gaidos, E. J., Henry, G. W., & Henry, S. M. 2000, AJ, 120, 1006

Gálvez, M. C., Montes, D., Fernández-Figueroa, M. J., & López-Santiago, J. 2006, Ap&SS, 304, 59

Gerbaldi, M., Faraggiana, R., & Balin, N. 2001, A&A, 379, 162

Gontcharov, G. A., Andronova, A. A., & Titov, O. A. 2000, A&A, 355, 1164

Goto, M. et al. 2002, ApJ, 567, L59

Gould, A. et al. 2006, ApJ, 644, L37

Gray, R. O., Corbally, C. J., Garrison, R. F., McFadden, M. T., & Robinson, P. E. 2003, AJ, 126, 2048

Greaves, J. S. et al. 1998, ApJ, 506, L133

Hahn, J. M., & Malhotra, R. 2005, AJ, 130, 2392

Haisch, Jr., K. E., Lada, E. A., & Lada, C. J. 2001, ApJ, 553, L153

Henry, T. J., Soderblom, D. R., Donahue, R. A., & Baliunas, S. L. 1996, AJ, 111, 439

Herriot, G. et al. 2000, in Proc. SPIE, Vol. 4007, Adaptive Optical Systems Technology, ed. P. L. Wizinowich, 115–125

Hinkley, S. et al. 2007, ApJ, 654, 633

Hodapp, K. W. et al. 2003, PASP, 115, 1388

Høg, E. et al. 1997, A&A, 323, L57

Høg, E. et al. 2000, A&A, 355, L27

Holland, W. S. et al. 1998, Nature, 392, 788

Huensch, M., Schmitt, J. H. M. M., & Voges, W. 1998, A&AS, 132, 155

Hünsch, M., Schmitt, J. H. M. M., Sterzik, M. F., & Voges, W. 1999, A&AS, 135, 319

Itoh, Y. et al. 2005, ApJ, 620, 984

Jayawardhana, R., Coffey, J., Scholz, A., Brandeker, A., & van Kerkwijk, M. H. 2006, ApJ, 648, 1206

Kalas, P., Graham, J. R., & Clampin, M. 2005, Nature, 435, 1067

Kirkpatrick, J. D., Dahn, C. C., Monet, D. G., Reid, I. N., Gizis, J. E., Liebert, J., & Burgasser, A. J. 2001, AJ, 121, 3235

Konacki, M., Torres, G., Jha, S., & Sasselov, D. D. 2003, Nature, 421, 507

Kotoneva, E., Flynn, C., Chiappini, C., & Matteucci, F. 2002, MNRAS, 336, 879

Lachaume, R., Dominik, C., Lanz, T., & Habing, H. J. 1999, A&A, 348, 897

Lafrenière, D., Marois, C., Doyon, R., Nadeau, D., & Artigau, E. 2007, ApJ, 660, 770

Levison, H. F., Morbidelli, A., Gomes, R., & Backman, D. 2007, in Protostars and Planets V, ed. B. Reipurth, D. Jewitt, & K. Keil, 669–684

López-Santiago, J., Montes, D., Crespo-Chacón, I., & Fernández-Figueroa, M. J. 2006, ApJ, 643, 1160

Lowrance, P. J. et al. 2005, AJ, 130, 1845

Luhman, K. L. 2004, ApJ, 614, 398

Luhman, K. L., Allers, K. N., Jaffe, D. T., Cushing, M. C., Williams, K. A., Slesnick, C. L., & Vacca, W. D. 2007a, ApJ, 659, 1629

Luhman, K. L., & Jayawardhana, R. 2002, ApJ, 566, 1132

Luhman, K. L. et al. 2007b, ApJ, 654, 570

Luhman, K. L. et al. 2006, ApJ, 649, 894

Macintosh, B. et al. 2006a, in Proc. SPIE, Vol. 6272, Advances in Adaptive Optics II, ed. B. L. Ellerbroek & D. Bonaccini Calia, 62720L

Macintosh, B. et al. 2006b, in Proc. SPIE, Vol. 6272, Advances in Adaptive Optics II, ed. B. L. Ellerbroek & D. Bonaccini Calia, 62720N

Makarov, V. V. 2006, AJ, 131, 2967

Makarov, V. V., & Kaplan, G. H. 2005, AJ, 129, 2420

Malhotra, R. 1995, AJ, 110, 420

Marcy, G., Butler, R. P., Fischer, D., Vogt, S., Wright, J. T., Tinney, C. G., & Jones, H. R. A. 2005, Progress of Theoretical Physics Supplement, 158, 24

Marley, M. S., Fortney, J. J., Hubickyj, O., Bodenheimer, P., & Lissauer, J. J. 2007, ApJ, 655, 541

Marois, C., Doyon, R., Nadeau, D., Racine, R., Riopel, M., Vallée, P., & Lafrenière, D. 2005, PASP, 117, 745

Marois, C., Doyon, R., Nadeau, D., Racine, R., & Walker, G. A. H. 2003, in EAS Publications Series, Vol. 8, Astronomy with High Contrast Imaging, ed. C. Aime & R. Soummer, 233–243

Marois, C., Doyon, R., Racine, R., & Nadeau, D. 2000, PASP, 112, 91

Marois, C., Lafrenière, D., Doyon, R., Macintosh, B., & Nadeau, D. 2006, ApJ, 641, 556

Marois, C., Macintosh, B., & Barman, T. 2007, ApJ, 654, L151

Martin, R. G., Lubow, S. H., Pringle, J. E., & Wyatt, M. C. 2007, ArXiv Astrophysics e-prints, arXiv:0704.3369 [astro-ph]

Masciadri, E., Mundt, R., Henning, T., Alvarez, C., & Barrado y Navascués, D. 2005, ApJ, 625, 1004

Matzner, C. D., & Levin, Y. 2005, ApJ, 628, 817

McCarthy, C., & Zuckerman, B. 2004, AJ, 127, 2871

Mohanty, S., & Basri, G. 2003, ApJ, 583, 451

Mohanty, S., Jayawardhana, R., Huélamo, N., & Mamajek, E. 2007, ApJ, 657, 1064

Montes, D., López-Santiago, J., Fernández-Figueroa, M. J., & Gálvez, M. C. 2001a, A&A, 379, 976

Montes, D., López-Santiago, J., Gálvez, M. C., Fernández-Figueroa, M. J., De Castro, E., & Cornide, M. 2001b, MNRAS, 328, 45

Nadal, R., Pedoussaut, A., Ginestet, N., & Carquillat, J.-M. 1974, A&A, 37, 191

Neuhäuser, R., Guenther, E. W., Wuchterl, G., Mugrauer, M., Bedalov, A., & Hauschildt, P. H. 2005, A&A, 435, L13

Nordström, B., Mayor, M., Andersen, J., Holmberg, J., Pont, F., Jørgensen, B. R., Olsen, E. H., Udry, S., & Mowlavi, N. 2004, A&A, 418, 989

Ochsenbein, F., Bauer, P., & Marcout, J. 2000, A&AS, 143, 23

Ozernoy, L. M., Gorkavyi, N. N., Mather, J. C., & Taidakova, T. A. 2000, ApJ, 537, L147

Perryman, M. A. C., & ESA. 1997, ESA SP Series, Vol. 1200, The HIPPARCOS and TYCHO catalogues. Astrometric and photometric star catalogues derived from the ESA HIPPARCOS Space Astrometry Mission (Noordwijk, Netherlands: ESA Publications Division)

Pollack, J. B., Hubickyj, O., Bodenheimer, P., Lissauer, J. J., Podolak, M., & Greenzweig, Y. 1996, Icarus, 124, 62

Potter, D., Martín, E. L., Cushing, M. C., Baudoz, P., Brandner, W., Guyon, O., & Neuhäuser, R. 2002, ApJ, 567, L133

Racine, R., Walker, G. A. H., Nadeau, D., Doyon, R., & Marois, C. 1999, PASP, 111, 587

Rasio, F. A., & Ford, E. B. 1996, Science, 274, 954

Reipurth, B., & Clarke, C. 2001, AJ, 122, 432

Rieke, G. H. et al. 2005, ApJ, 620, 1010

Saffe, C., Gómez, M., & Chavero, C. 2005, A&A, 443, 609

Santos, N. C., Israelian, G., & Mayor, M. 2004, A&A, 415, 1153

Schneider, G., & Silverstone, M. D. 2003, in Proc. SPIE, Vol. 4860, High-Contrast Imaging for Exo-Planet Detection, ed. A. B. Schultz, 1–9

Schneider, G. et al. 1999, ApJ, 513, L127

Seifahrt, A., Neuhäuser, R., & Hauschildt, P. H. 2007, A&A, 463, 309

Shen, S., & Wadsley, J. 2006, ApJ, 651, L145

Sivia, D. S. 1996, Data Analysis: A Bayesian Tutorial (Oxford Science Publications) (Oxford University Press)

Soderblom, D. R., & Mayor, M. 1993, AJ, 105, 226

Song, I., Caillault, J.-P., Barrado y Navascués, D., Stauffer, J. R., & Randich, S. 2000, ApJ, 533, L41

Song, I., Zuckerman, B., & Bessell, M. S. 2004, ApJ, 614, L125

Sousa, S. G., Santos, N. C., Israelian, G., Mayor, M., & Monteiro, M. J. P. F. G. 2006, A&A, 458, 873

Sparks, W. B., & Ford, H. C. 2002, ApJ, 578, 543

Takeda, Y., & Kawanomoto, S. 2005, PASJ, 57, 45

Taylor, B. J. 2005, ApJS, 161, 444

Tsiganis, K., Gomes, R., Morbidelli, A., & Levison, H. F. 2005, Nature, 435, 459

Udalski, A. et al. 2005, ApJ, 628, L109

Udry, S., Fischer, D., & Queloz, D. 2007, in Protostars and Planets V, ed. B. Reipurth, D. Jewitt, & K. Keil, 685–699

Valdes, F., Gupta, R., Rose, J. A., Singh, H. P., & Bell, D. J. 2004, ApJS, 152, 251

Valenti, J. A., & Fischer, D. A. 2005, ApJS, 159, 141

Veras, D., & Armitage, P. J. 2004, MNRAS, 347, 613

Weidenschilling, S. J., & Marzari, F. 1996, Nature, 384, 619

Weinberger, A. J., Becklin, E. E., Schneider, G., Smith, B. A., Lowrance, P. J., Silverstone, M. D., Zuckerman, B., & Terrile, R. J. 1999, ApJ, 525, L53

Weis, E. W. 1991, AJ, 101, 1882

Whitworth, A. P., & Stamatellos, D. 2006, A&A, 458, 817

Wichmann, R., Schmitt, J. H. M. M., & Hubrig, S. 2003, A&A, 399, 983

Wielen, R., Dettbarn, C., Jahreiß, H., Lenhardt, H., Schwan, H., & Jährling, R. 2000, in IAU Symposium, 144P–+

Wilner, D. J., Holman, M. J., Kuchner, M. J., & Ho, P. T. P. 2002, ApJ, 569, L115

Wright, J. T., Marcy, G. W., Butler, R. P., & Vogt, S. S. 2004, ApJS, 152, 261

Wyatt, M. C., Greaves, J. S., Dent, W. R. F., & Coulson, I. M. 2005, ApJ, 620, 492

Zuckerman, B., Bessell, M. S., Song, I., & Kim, S. 2006, ApJ, 649, L115

Zuckerman, B., & Song, I. 2004a, ApJ, 603, 738

—. 2004b, ARA&A, 42, 685

Zuckerman, B., Song, I., & Bessell, M. S. 2004, ApJ, 613, L65

Zuckerman, B., Song, I., Bessell, M. S., & Webb, R. A. 2001, ApJ, 562, L87

This preprint was prepared with the AAS LaTeX macros v5.2.

Table 1. GDPS target sample

| Names HD | GJ | HIP | Other | $\alpha$ (J2000) | $\delta$ (J2000) | Spectral Type | H (mag) | Dist.[a] (pc) | $\mu_\alpha \cos\delta$[a] (mas/yr) | $\mu_\delta$[a] (mas/yr) | [Fe/H] | [Fe/H] Ref. | Age (Myr) | Age Ref. | Notes |
|---|---|---|---|---|---|---|---|---|---|---|---|---|---|---|---|
| 166 | 5 | 544 | - | $00^h06^m36^s.78$ | $+29°01'17''.4$ | K0 V | 4.63 | 13.7 | 379.9 | −178.3 | 0.18 | V05 | 150–300 | G98,G00,F04,L06 | Her |
| 691 | - | 919 | V344 And | $00^h11^m22^s.44$ | $+30°26'58''.5$ | K0 V | 6.26 | 34.1 | 210.7 | 35.3 | 0.32 | V05 | 50–280 | W03,W04,C05 | - |
| 1405 | - | - | PW And | $00^h18^m20^s.90$ | $+30°57'22''.0$ | K2 V | 6.51 | 30.6[b] | 143.7[b] | −171.5[b] | -0.78 | N04 | 50–50 | Z04b | AB Dor |
| 5996 | - | 4907 | - | $01^h02^m57^s.22$ | $+69°13'37''.4$ | G5 V | 5.98 | 25.8 | 223.9 | −148.4 | -0.28 | K02 | 100–650 | M01a,G03 | - |
| 9540 | 59A | 7235 | - | $01^h33^m15^s.81$ | $-24°10'40''.7$ | K0 V | 5.27 | 19.5 | 271.9 | −159.5 | -0.02 | V05 | 100–1350 | M01a,W04 | - |
| 10008 | - | 7576 | - | $01^h37^m35^s.47$ | $-06°45'37''.5$ | G5 V | 5.90 | 23.6 | 171.0 | −97.7 | - | - | 150–300 | F04,L06 | Her |
| - | 82 | 9291 | V596 Cas | $01^h59^m23^s.51$ | $+58°31'16''.1$ | dM4e | 7.22 | 12.0 | 321.8 | −195.3 | - | - | 50–50 | M06 | $\alpha$ Per |
| 14802 | 97 | 11072 | kap For | $02^h22^m32^s.55$ | $-23°48'58''.8$ | G2 V | 3.71 | 21.9 | 197.3 | −4.4 | -0.04 | T05b | 5000–6700 | L99,W04,B99 | m |
| 16765 | - | 12530 | 84 Cet | $02^h41^m14^s.00$ | $-00°41'44''.4$ | F7 V | 4.64 | 21.6 | 218.9 | −125.3 | -0.27 | N04 | 100–400 | M01a,H98,F95 | m |
| 17190 | 112 | 12926 | - | $02^h46^m15^s.21$ | $+25°38'59''.6$ | K1 V | 6.00 | 25.7 | 238.7 | −149.9 | -0.11 | V05 | 50–3500 | M01a,W04 | - |
| 17382 | 113 | 13081 | - | $02^h48^m09^s.14$ | $+27°04'07''.1$ | K1 V | 5.69 | 22.4 | 264.2 | −127.8 | 0.12 | T05b | 50–600 | M01a,W04 | - |
| 17925 | 117 | 13402 | EP Eri | $02^h52^m32^s.13$ | $-12°46'11''.0$ | K2 V | 4.23 | 10.4 | 398.1 | −189.6 | 0.18 | V05 | 40–128 | W03,M01a,M01b,L99 | LA |
| 18803 | 120.2 | 14150 | 51 Ari | $03^h02^m26^s.03$ | $+26°36'33''.3$ | G8 V | 5.02 | 21.2 | 234.2 | −168.2 | 0.11 | V05 | 800–3600 | W04,T05a | - |
| 19994 | 128 | 14954 | 94 Cet | $03^h12^m46^s.44$ | $-01°11'46''.0$ | F8 V | 3.77 | 22.4 | 193.4 | −69.2 | 0.19 | V05 | 800–3500 | W04,T05a | m |
| 20367 | - | 15323 | - | $03^h17^m40^s.05$ | $+31°07'37''.4$ | G0 V | 5.12 | 27.1 | −103.1 | −56.6 | 0.17 | S04a | 50–150 | W03 | - |
| - | - | - | 2E 759 | $03^h20^m49^s.50$ | $-19°16'10''.0$ | K7 V | 7.66 | 27.0 | 90.8 | −43.8 | - | - | 50–150 | L06 | - |
| 22049 | 144 | 16537 | eps Eri | $03^h32^m55^s.84$ | $-09°27'29''.7$ | K2 V | 1.88 | 3.2 | −976.4 | 18.0 | -0.03 | V05 | 530–930 | S00 | - |
| - | - | 17695 | - | $03^h47^m23^s.35$ | $-01°58'19''.9$ | M3e | 7.17 | 16.3 | 186.7 | −271.8 | - | - | 80–120 | L06 | LA (B4) |
| 25457 | 159 | 18859 | - | $04^h02^m36^s.74$ | $-00°16'08''.1$ | F6 V | 4.34 | 19.2 | 151.2 | −252.0 | 0.02 | T05b | 80–120 | L06 | LA (B4) |
| 283750 | 171.2 | 21482 | V833 Tau | $04^h36^m48^s.24$ | $+27°07'55''.9$ | K2 V | 5.40 | 17.9 | 232.4 | −147.1 | - | - | 50–150 | W03 | - |
| 30652 | 178 | 22449 | 1 Ori | $04^h49^m50^s.41$ | $+06°57'40''.6$ | F6 V | 1.76 | 8.0 | 463.4 | 11.6 | 0.03 | V05 | 50–500 | M01a,H99 | - |
| - | 182 | 23200 | V1005 Ori | $04^h59^m34^s.83$ | $+01°47'00''.7$ | M1 V | 6.45 | 26.7 | 37.1 | −93.9 | - | - | 10–50 | F98,B99 | - |
| - | 234A | 30920 | V577 Mon | $06^h29^m23^s.40$ | $-02°48'50''.3$ | M4 | 5.75 | 4.1 | 694.7 | −618.6 | - | - | 100–3000 | M01a,M03 | m |
| - | 281 | 37288 | - | $07^h39^m23^s.04$ | $+02°11'01''.2$ | K7 | 6.09 | 14.9 | −147.9 | −246.6 | - | - | 150–300 | L06 | Her |
| - | 285 | 37766 | YZ CMi | $07^h44^m40^s.17$ | $+03°33'08''.8$ | M4.5 V | 6.01 | 5.9 | −344.9 | −450.8 | - | - | 50–50 | Z | - |
| 72905 | 311 | 42438 | 3 Uma | $08^h39^m11^s.70$ | $+65°01'15''.3$ | G1.5 V | 4.28 | 14.3 | −27.7 | 87.9 | -0.09 | T05b | 300–300 | S93,M01b | U Ma |
| 75332 | - | 43410 | - | $08^h50^m32^s.22$ | $+33°17'06''.2$ | F7 Vn | 5.04 | 28.7 | −62.2 | −85.0 | 0.14 | V05 | 50–150 | W03 | - |
| 77407 | - | 44458 | - | $09^h03^m27^s.08$ | $+37°50'27''.5$ | G0 | 5.53 | 30.1 | −86.3 | −168.8 | 0.10 | V05 | 10–50 | W03,M01a,M01b | LA,m |
| 78141 | - | - | - | $09^h07^m18^s.08$ | $+22°52'21''.6$ | K0 V | 5.92 | 21.4[c] | −0.4[d] | −67.6[d] | - | - | 50–150 | W03 | - |
| 82558 | 355 | 46816 | LQ Hya | $09^h32^m25^s.57$ | $-11°11'04''.7$ | K0 V | 5.60 | 18.3 | −248.2 | 35.1 | 0.33 | V05 | 50–100 | W03,M01b | - |
| 82443 | 354.1 | 46843 | DX Leo | $09^h32^m43^s.76$ | $+26°59'18''.7$ | K0 V | 5.24 | 17.7 | −147.5 | −246.3 | -0.10 | T05b | 50–150 | W03,M01b | LA |
| - | 393 | 51317 | - | $10^h28^m55^s.55$ | $+00°50'27''.6$ | M2 | 5.61 | 7.2 | −602.3 | −731.9 | - | - | 80–120 | L06 | LA (B4) |
| 90905 | - | 51386 | - | $10^h29^m42^s.23$ | $+01°29'28''.0$ | F5 | 5.60 | 31.6 | −151.4 | −125.3 | 0.07 | V05 | 50–150 | W03 | - |
| 91901 | - | 51931 | - | $10^h36^m30^s.79$ | $-13°50'35''.8$ | K2 V | 6.64 | 31.6 | −164.6 | 23.8 | -0.03 | K02 | 50–5000 | M01a | - |
| 92945 | 3615 | 52462 | - | $10^h43^m28^s.27$ | $-29°03'51''.4$ | K1 V | 5.77 | 21.6 | −215.4 | −48.5 | 0.13 | V05 | 80–120 | L06,W03,S04b,W04 | LA (B4) |
| 93528 | - | 52787 | - | $10^h47^m31^s.16$ | $-22°20'52''.9$ | K0 V | 6.56 | 34.9 | −122.7 | −29.4 | 0.11 | K02 | 50–150 | W03,S02 | - |
| - | 402 | 53020 | EE Leo | $10^h50^m52^s.06$ | $+06°48'29''.3$ | M4 | 6.71 | 5.6 | −804.4 | −809.6 | - | - | 150–300 | L06 | Her |
| 96064 | - | 54155 | - | $11^h04^m41^s.47$ | $-04°13'15''.9$ | G4 | 5.90 | 24.6 | −178.0 | −104.1 | -0.01 | T05b | 50–150 | W03 | m |
| 97334 | 417 | 54745 | - | $11^h12^m32^s.35$ | $+35°48'50''.7$ | G0 V | 5.02 | 21.7 | −248.6 | −151.3 | 0.09 | V05 | 80–300 | K01 | - |
| 102195 | - | 57370 | - | $11^h45^m42^s.29$ | $+02°49'17''.3$ | K0 V | 6.27 | 29.0 | −190.3 | −111.4 | 0.05 | S06 | 100–5000 | M01a | - |
| 102392 | - | 57494 | - | $11^h47^m03^s.83$ | $-11°49'26''.6$ | K2 | 6.36 | 24.6 | −206.3 | −60.7 | - | - | 100–5000 | M01a | m |
| 105631 | 3706 | 59280 | - | $12^h09^m37^s.26$ | $+40°15'07''.4$ | K0 V | 5.70 | 24.3 | −314.0 | −51.3 | 0.20 | V05 | 1600–1600 | M01b,W04 | - |
| 107146 | - | 60074 | - | $12^h19^m06^s.50$ | $+16°32'53''.9$ | G2 V | 5.61 | 28.5 | −175.7 | −148.3 | -0.03 | V05 | 50–100 | W03,Z04a | - |
| 108767B | - | - | del Crv B | $12^h29^m51^s.85$ | $-16°30'55''.6$ | K0 V | 6.37 | 26.9 | −210.0 | −139.3 | - | - | 40–260 | R05,G01,M01a | LA |
| 109085 | 471.2 | 61174 | eta Crv | $12^h32^m04^s.23$ | $-16°11'45''.6$ | F2 V | 3.37 | 18.2 | −424.4 | −58.4 | -0.05 | N04 | 600–1300 | M03,W05 | - |
| - | - | - | BD+60 1417 | $12^h43^m33^s.28$ | $+60°00'52''.7$ | K0 | 7.36 | 17.7[c] | −125.2[d] | −66.4[d] | - | - | 50–150 | W03 | - |
| 111395 | 486.1 | 62523 | - | $12^h48^m47^s.05$ | $+24°50'24''.8$ | G5 V | 4.71 | 17.2 | −334.6 | −106.1 | 0.13 | V05 | 600–1200 | H99,W04,T05a | - |
| 113449 | - | 63742 | - | $13^h03^m49^s.65$ | $-05°09'42''.5$ | G5 V | 5.67 | 22.1 | −189.8 | −219.6 | -0.22 | T05b | 80–120 | L06 | LA (B4) |
| - | 507.1 | 65016 | - | $13^h19^m40^s.12$ | $+33°20'47''.5$ | M1.5 | 6.64 | 17.4 | −298.8 | −143.9 | - | - | 100–5000 | M01a | - |
| 116956 | - | 65515 | - | $13^h25^m45^s.53$ | $+56°58'13''.8$ | G9 V | 5.48 | 21.9 | −217.4 | 11.2 | 0.06 | T05b | 100–500 | M01a,G00 | - |

Table 1—Continued

| Names | | | | $\alpha$ | $\delta$ | Spectral | H | Dist.[a] | $\mu_\alpha \cos\delta$[a] | $\mu_\delta$[a] | [Fe/H] | [Fe/H] | Age | Age | Notes |
|---|---|---|---|---|---|---|---|---|---|---|---|---|---|---|---|
| HD | GJ | HIP | Other | (J2000) | (J2000) | Type | (mag) | (pc) | (mas/yr) | (mas/yr) | | Ref. | (Myr) | Ref. | |
| 118100 | 517 | 66252 | EQ Vir | $13^h34^m43^s.21$ | $-08°20'31''.3$ | K5 Ve | 6.31 | 19.8 | −287.4 | −91.0 | 0.00 | C97 | 50–50 | L05 | - |
| - | 524.1 | 67092 | - | $13^h45^m05^s.34$ | $-04°37'13''.2$ | K5 | 7.33 | 25.7 | −159.9 | −95.3 | - | - | 100–5000 | M01a | - |
| 124106 | 3827 | 69357 | - | $14^h11^m46^s.17$ | $-12°36'42''.4$ | K1 V | 5.95 | 23.1 | −257.5 | −179.5 | -0.10 | V05 | 800–1500 | H99,M01a,W04 | - |
| 125161B | 9474B | - | - | $14^h16^m12^s.16$ | $+51°22'34''.7$ | K1 | 6.32 | 29.8 | −150.0 | 89.4 | - | - | 50–5000 | M01a | - |
| 129333 | 559.1 | 71631 | EK Dra | $14^h39^m00^s.21$ | $+64°17'30''.0$ | G0 V | 6.01 | 33.9 | −138.6 | −11.9 | 0.16 | V05 | 20–120 | M01b,W03,L06 | LA (B4),m |
| 130004 | - | 72146 | - | $14^h45^m24^s.18$ | $+13°50'46''.7$ | K0 V | 5.67 | 19.5 | −232.9 | −225.7 | -0.24 | K02 | 100–5000 | M01a | - |
| 130322 | - | 72339 | - | $14^h47^m32^s.73$ | $-00°16'53''.3$ | K0 V | 6.32 | 29.8 | −129.6 | −140.8 | 0.01 | V05 | 770–2400 | W04,S05 | - |
| 130948 | 564 | 72567 | - | $14^h50^m15^s.81$ | $+23°54'42''.6$ | G1 V | 4.69 | 17.9 | 144.7 | 32.4 | 0.05 | V05 | 50–150 | W03 | - |
| 135363 | - | 74045 | - | $15^h07^m56^s.26$ | $+76°12'02''.7$ | G5 | 6.33 | 29.4 | −131.9 | 169.3 | -0.10 | K02 | 35–100 | W03,M01a,C05 | IC 2391,m |
| 139813 | - | 75829 | - | $15^h29^m23^s.59$ | $+80°27'01''.0$ | G5 | 5.56 | 21.7 | −217.4 | 105.5 | 0.14 | V05 | 50–150 | W03 | - |
| 141272 | 3917 | 77408 | - | $15^h48^m09^s.46$ | $+01°34'18''.3$ | G8 V | 5.61 | 21.3 | −176.2 | −166.7 | -0.08 | T05b | 150–340 | G98,G00,W04,L06 | - |
| 147379B | 617B | 79762 | EW Dra | $16^h16^m45^s.31$ | $+67°15'22''.5$ | M3 | 6.30 | 10.7 | −485.6 | 90.7 | 0.00 | V04 | 100–1000 | M01a, H99 | - |
| - | 628 | 80824 | V2306 Oph | $16^h30^m18^s.06$ | $-12°39'45''.3$ | M3.5 | 5.37 | 4.3 | −93.6 | −1184.9 | -0.25 | C01 | 100–5000 | M01a | LA |
| - | - | 81084 | - | $16^h33^m41^s.61$ | $-09°33'12''.0$ | M0.5 | 7.78 | 31.9 | −67.4 | −179.7 | - | - | 80–120 | L06 | LA (B4) |
| 160934 | 4020A | 86346 | - | $17^h38^m39^s.63$ | $+61°14'16''.1$ | K7 | 7.00 | 24.5 | −31.2 | 59.4 | - | - | 30–50 | Z04c,L06 | AB Dor,m |
| 162283 | 696 | 87322 | - | $17^h50^m34^s.03$ | $-06°03'01''.0$ | M0 | 6.70 | 21.9 | −26.1 | −131.4 | - | - | 100–5000 | M01a, B98 | - |
| 166181 | - | 88848 | V815 Her | $18^h08^m16^s.03$ | $+29°41'28''.1$ | G6 V | 5.76 | 32.3[e] | 107.0[e] | −31.0[e] | -0.70 | N04 | 50–150 | W03 | m |
| 167605 | - | 89005 | LP Dra | $18^h09^m55^s.50$ | $+69°40'49''.8$ | K2 V | 6.46 | 31.0 | −25.3 | 193.9 | 0.13 | K02 | 50–5000 | M01a | m |
| 187748 | - | 97438 | - | $19^h48^m15^s.45$ | $+59°25'22''.4$ | G0 | 5.32 | 28.4 | 15.8 | 116.5 | -0.06 | N04 | 50–150 | W03 | - |
| - | 791.3 | 101262 | - | $20^h31^m32^s.07$ | $+33°46'33''.1$ | K5 V | 6.64 | 26.2 | 142.1 | 16.6 | - | - | 50–1000 | M01a,H99 | - |
| 197481 | 803 | 102409 | AU Mic | $20^h45^m09^s.53$ | $-31°20'27''.2$ | M0 | 4.83 | 9.9 | 280.4 | −360.1 | - | - | 8–20 | Z01 | $\beta$ Pic |
| 201651 | - | 104225 | - | $21^h06^m56^s.39$ | $+69°40'28''.5$ | K0 | 6.41 | 32.8 | 109.0 | 66.0 | -0.18 | K02 | 50–5900 | M01a,W04 | - |
| 202575 | 824 | 105038 | - | $21^h16^m32^s.47$ | $+09°23'37''.8$ | K3 V | 5.53 | 16.2 | 146.5 | −119.1 | 0.04 | V05 | 100–1000 | M01a,H99 | - |
| - | 4199 | 106231 | LO Peg | $21^h31^m01^s.71$ | $+23°20'07''.4$ | K8 | 6.52 | 25.1 | 134.1 | −144.8 | - | - | 30–50 | Z04c,L06 | AB Dor |
| 206860 | 836.7 | 107350 | HN Peg | $21^h44^m31^s.33$ | $+14°46'19''.0$ | G0 V | 4.60 | 18.4 | 231.1 | −113.5 | -0.02 | V05 | 150–300 | L06,G98,G00 | Her |
| 208313 | 840 | 108156 | - | $21^h54^m45^s.04$ | $+32°19'42''.9$ | K0 V | 5.68 | 20.3 | 210.6 | −233.4 | -0.04 | V05 | 100–1000 | M01a,H99 | - |
| - | - | - | V383 Lac | $22^h20^m07^s.03$ | $+49°30'11''.8$ | K1 V | 6.58 | 27.5[b] | 93.4[b] | 5.0[b] | - | - | 50–150 | W03,M01a,C05 | - |
| 213845 | 863.2 | 111449 | ups Aqr | $22^h34^m41^s.64$ | $-20°42'29''.6$ | F7 V | 4.27 | 22.7 | 221.6 | −146.6 | 0.11 | T05b | 150–300 | L06 | Her,m |
| - | 875.1 | 112909 | GT Peg | $22^h51^m53^s.54$ | $+31°45'15''.2$ | M3 | 7.13 | 14.2 | 527.0 | −50.6 | - | - | 200–300 | L05 | - |
| - | 876 | 113020 | IL Aqr | $22^h53^m16^s.73$ | $-14°15'49''.3$ | M4 | 5.35 | 4.7 | 960.3 | −675.6 | - | - | 100–5000 | M01a | - |
| - | 9809 | 114066 | - | $23^h06^m04^s.84$ | $+63°55'34''.4$ | M0 | 7.17 | 24.9 | 171.0 | −58.5 | - | - | 30–50 | Z04c,L06 | AB Dor |
| 220140 | - | 115147 | V368 Cep | $23^h19^m26^s.63$ | $+79°00'12''.7$ | K1 V | 5.51 | 19.7 | 201.3 | 71.6 | -0.64 | N04 | 50–150 | M01b,W03 | LA,m |
| 221503 | 898A | 116215 | - | $23^h32^m49^s.40$ | $-16°50'44''.3$ | K5 | 5.61 | 13.9 | 343.6 | −217.7 | 0.00 | C04 | 100–800 | M01a,H99 | - |
| - | 900 | 116384 | - | $23^h35^m00^s.28$ | $+01°36'19''.5$ | K7 | 6.28 | 19.3 | 343.0 | 26.8 | -0.10 | C01 | 150–250 | Z06 | Ca,m |
| - | 907.1 | 117410 | - | $23^h48^m25^s.69$ | $-12°59'14''.8$ | K8 | 6.49 | 27.1 | 233.6 | 22.1 | - | - | 150–250 | Z06 | Ca,m |

[a]From the Hipparcos catalog (Perryman & ESA 1997), unless stated otherwise.

[b]From Montes et al. (2001b).

[c]From the Tycho catalog (Høg et al. 1997).

[d]From the Tycho-2 catalog (Høg et al. 2000).

[e]From Fekel et al. (2005).

Note. — Star is a member of ($\alpha$ Per) $\alpha$ Persei; (AB Dor) AB Doradus; ($\beta$ Pic) $\beta$ Pictoris; (Ca-Near) Carina-Near; (Her-Lyr) Hercules-Lyra; (LA) Local association; (LA (B4)) Local association, subgroup B4; (U Ma) Ursa Major. "m" indicates that the star is a multiple.

References. — (B99) Barrado y Navascués et al. 1999; (C05) Carpenter et al. 2005; (C01) Cayrel de Strobel et al. 2001; (C97) Cayrel de Strobel et al. 1997; (C04) Clem et al. 2004; (F95) Favata et al. 1995; (F98) Favata et al. 1998; (F04) Fuhrmann 2004; (G00) Gaidos et al. 2000; (G98) Gaidos 1998; (G01) Gerbaldi et al. 2001; (G03) Gray et al. 2003; (H98) Huensch et al. 1998; (H99) Hünsch et al. 1999; (K01) Kirkpatrick et al. 2001; (K02) Kotoneva et al. 2002; (L99) Lachaume et al. 1999; (L06) López-Santiago et al. 2006; (L05) Lowrance et al. 2005; (M06) Makarov 2006; (M03) Mohanty & Basri 2003; (M01a) Montes et al. 2001b; (M01b) Montes et al. 2001a; (N04) Nordström et al. 2004; (R05) Rieke et al. 2005; (S05) Saffe et al. 2005; (S04a) Santos et al. 2004; (S93) Soderblom & Mayor 1993; (S00) Song et al. 2000; (S04b) Song et al. 2004; (S06) Sousa et al. 2006; (T05a) Takeda & Kawanomoto 2005; (T05b) Taylor 2005; (V04) Valdes et al. 2004; (V05) Valenti & Fischer 2005; (W03) Wichmann et al. 2003; (W04) Wright et al. 2004; (W05) Wyatt et al. 2005; (Z01) Zuckerman et al. 2001; (Z04b) Zuckerman & Song 2004b; (Z04a) Zuckerman & Song 2004a; (Z04c) Zuckerman et al. 2004; (Z06) Zuckerman et al. 2006; (Z) B. Zuckerman, private communication.

Table 2. GDPS observation log

| Name | Date | Number of exposures | Strehl (%) | FOV rotation (deg) | Saturation radius (″) |
|---|---|---|---|---|---|
| HD 166 | 2005/08/25 | 83 | 5-8 | 55 | 1.0 |
| | 2006/07/18 | 83 | 7-10 | 81 | 0.8 |
| HD 691 | 2005/08/10 | 90 | 13-17 | 70 | 0.5 |
| | 2006/09/18 | 117 | 16-30 | 88 | 0.5 |
| HD 1405 | 2004/08/22 | 90 | 4-10 | 17 | 0.5 |
| | 2005/08/04 | 90 | 6-18 | 69 | 0.4 |
| HD 5996 | 2005/08/12 | 90 | 18-20 | 24 | 0.5 |
| | 2006/09/25 | 90 | 15-17 | 21 | 0.5 |
| HD 9540 | 2005/08/14 | 90 | 16-19 | 25 | 0.6 |
| | 2006/09/28 | 45 | 14-17 | 11 | 0.6 |
| HD 10008 | 2005/08/10 | 90 | 18-20 | 36 | 0.5 |
| GJ 82 | 2005/08/31 | 90 | 10-12 | 27 | 0.3 |
| HD 14802 | 2005/08/20 | 90 | - | 23 | 1.1 |
| HD 16765 | 2005/09/10 | 90 | 14-17 | 45 | 0.7 |
| HD 17190 | 2005/08/24 | 90 | 13-30 | 108 | 0.5 |
| HD 17382 | 2004/12/22 | 66 | 15 | 68 | 0.6 |
| | 2005/09/11 | 90 | 19-23 | 104 | 0.5 |
| HD 17925 | 2004/11/04 | 83 | $\gtrsim 18^{a}$ | 29 | 0.7 |
| HD 18803 | 2004/12/24 | 90 | 7-14 | 99 | 0.7 |
| | 2005/09/12 | 78 | 17-18 | 108 | 0.7 |
| HD 19994 | 2005/08/31 | 90 | - | 44 | 0.9 |
| | 2006/10/01 | 57 | - | 27 | 0.7 |
| HD 20367 | 2005/10/02 | 90 | 12-14 | 67 | 0.7 |
| 2E 759 | 2005/10/17 | 59 | 7-10 | 31 | 0.3 |
| HD 22049 | 2005/09/08 | 90 | - | 32 | 2.1 |
| HIP 17695 | 2005/09/13 | 89 | 20-20 | 45 | 0.3 |
| HD 25457 | 2005/10/02 | 90 | - | 43 | 1.0 |
| HD 283750 | 2004/10/24 | 90 | 15 | 99 | 0.6 |
| | 2005/10/04 | 87 | 19-23 | 101 | 0.6 |
| HD 30652 | 2005/09/12 | 52 | - | 35 | 1.9 |
| GJ 182 | 2004/11/05 | 90 | 16-20 | 31 | 0.4 |
| | 2005/10/17 | 33 | 11-11 | 29 | 0.4 |
| GJ 234A | 2005/11/05 | 72 | 16 | 34 | 0.4 |
| GJ 281 | 2005/03/25 | 67 | 9-10 | 49 | 0.6 |
| | 2006/02/12 | 25 | 8-9 | 11 | 0.5 |
| GJ 285 | 2005/03/18 | 20 | - | 10 | 0.5 |
| | 2006/02/12 | 90 | 4-5 | 73 | 0.6 |
| HD 72905 | 2005/04/23 | 84 | 7 | 25 | 0.9 |
| HD 75332 | 2005/04/24 | 89 | $\gtrsim 17^{a}$ | 27 | 0.6 |
| | 2006/12/20 | 16 | $\gtrsim 16^{a}$ | 11 | 0.6 |
| HD 77407 | 2005/04/26 | 84 | 16-19 | 33 | 0.6 |
| HD 78141 | 2004/12/21 | 85 | 14-16 | 19 | 0.6 |
| HD 82558 | 2005/04/18 | 90 | - | 30 | 0.6 |
| HD 82443 | 2004/12/25 | 75 | 18 | 28 | 0.6 |
| GJ 393 | 2005/04/20 | 90 | 13-15 | 44 | 0.5 |

Table 2—Continued

| Name | Date | Number of exposures | Strehl (%) | FOV rotation (deg) | Saturation radius (″) |
|---|---|---|---|---|---|
| HD 90905 | 2005/03/18 | 90 | 13-18 | 47 | 0.6 |
| | 2006/04/11 | 35 | 13-15 | 14 | 0.6 |
| HD 91901 | 2005/04/29 | 71 | 9 | 22 | 0.5 |
| HD 92945 | 2005/05/26 | 85 | 15-16 | 19 | 0.6 |
| | 2006/05/16 | 10 | 10-11 | 2 | 1.1 |
| HD 93528 | 2005/04/30 | 86 | - | 26 | 0.4 |
| GJ 402 | 2005/04/26 | 79 | 12-16 | 37 | 0.4 |
| | 2006/02/16 | 60 | 6-10 | 33 | 0.4 |
| HD 96064 | 2005/04/19 | 89 | 21-23 | 37 | 0.5 |
| | 2006/03/05 | 90 | 13-19 | 36 | 0.5 |
| HD 97334 | 2005/04/18 | 90 | 16-17 | 54 | 0.7 |
| HD 102195 | 2005/04/24 | 91 | 20-21 | 54 | 0.4 |
| | 2006/03/18 | 82 | 12-18 | 30 | 0.4 |
| HD 102392 | 2005/04/23 | 89 | 19-24 | 32 | 0.4 |
| | 2006/03/12 | 90 | 9-13 | 31 | 0.4 |
| HD 105631 | 2005/05/29 | 90 | 14-19 | 45 | 0.6 |
| HD 107146 | 2005/05/30 | 90 | 21-26 | 71 | 0.6 |
| HD 108767B | 2005/04/22 | 90 | 14 | 27 | 0.5 |
| | 2006/02/16 | 43 | 10-11 | 14 | 0.4 |
| HD 109085 | 2005/05/26 | 90 | - | 22 | 1.1 |
| | 2006/03/12 | 15 | - | 3 | 1.1 |
| BD+60 1417 | 2005/04/18 | 90 | 18-23 | 24 | 0.3 |
| | 2006/04/11 | 63 | 12 | 19 | 0.3 |
| HD 111395 | 2005/04/19 | 89 | $\gtrsim 12^{a}$ | 120 | 0.8 |
| HD 113449 | 2005/06/01 | 47 | 10-20 | 37 | 0.5 |
| GJ 507.1 | 2005/06/07 | 87 | 5-7 | 61 | 0.5 |
| HD 116956 | 2005/05/29 | 90 | 5-14 | 27 | 0.5 |
| | 2006/05/16 | 60 | 5-8 | 18 | 0.6 |
| HD 118100 | 2005/04/27 | 53 | - | 18 | 0.4 |
| GJ 524.1 | 2005/04/18 | 90 | 18-25 | 37 | 0.3 |
| | 2006/05/18 | 90 | 13-14 | 37 | 0.3 |
| HD 124106 | 2005/04/19 | 86 | 18-19 | 32 | 0.5 |
| | 2006/02/16 | 80 | 10-12 | 24 | 0.5 |
| HD 125161B | 2005/05/30 | 90 | 17-23 | 31 | 0.4 |
| HD 129333 | 2005/04/20 | 90 | 19-20 | 22 | 0.5 |
| HD 130004 | 2005/05/25 | 90 | 17-18 | 105 | 0.6 |
| HD 130322 | 2005/05/27 | 88 | 15-19 | 40 | 0.5 |
| | 2006/05/15 | 10 | 10-10 | 5 | 0.6 |
| HD 130948 | 2005/04/17 | 90 | $\gtrsim 9^{a}$ | 122 | 0.9 |
| HD 135363 | 2005/04/18 | 87 | 14-15 | 19 | 0.5 |
| | 2006/02/16 | 60 | 8-9 | 14 | 0.5 |
| HD 139813 | 2005/05/30 | 90 | $\gtrsim 12^{a}$ | 20 | 0.6 |
| HD 141272 | 2005/04/19 | 90 | 18-19 | 47 | 0.6 |
| | 2006/03/12 | 42 | 13 | 20 | 0.6 |
| HD 147379B | 2005/04/18 | 90 | 17-17 | 22 | 0.5 |

Table 2—Continued

| Name | Date | Number of exposures | Strehl (%) | FOV rotation (deg) | Saturation radius (″) |
|---|---|---|---|---|---|
| GJ 628 | 2005/04/17 | 90 | 11 | 29 | 0.7 |
| | 2006/04/11 | 40 | 9-14 | 13 | 0.7 |
| HIP 81084 | 2005/04/19 | 73 | 17-18 | 30 | 0.3 |
| | 2006/05/15 | 90 | 8-13 | 31 | 0.3 |
| HD 160934 | 2005/04/18 | 84 | 17-24 | 24 | 0.4 |
| | 2006/09/17 | 14 | 12-14 | 4 | 0.6 |
| HD 162283 | 2005/04/20 | 120 | 15-19 | 45 | 0.4 |
| | 2006/09/16 | 100 | 27-29 | 31 | 0.3 |
| HD 166181 | 2005/04/17 | 90 | 16 | 76 | 0.6 |
| | 2006/09/18 | 45 | 18-21 | 37 | 0.5 |
| HD 167605 | 2005/05/27 | 90 | 20 | 22 | 0.4 |
| HD 187748 | 2005/05/25 | 97 | 15-19 | 30 | 0.7 |
| | 2006/09/15 | 75 | $\gtrsim 22$[a] | 21 | 0.5 |
| GJ 791.3 | 2005/05/26 | 87 | 9-19 | 54 | 0.4 |
| HD 197481 | 2005/07/29 | 68 | 6-10 | 21 | 0.9 |
| HD 201651 | 2005/06/27 | 90 | 18-23 | 21 | 0.4 |
| | 2006/09/14 | 30 | 19-21 | 7 | 0.4 |
| HD 202575 | 2005/07/16 | 90 | 17-23 | 75 | 0.6 |
| | 2006/09/14 | 30 | 16-18 | 9 | 0.6 |
| GJ 4199 | 2004/08/23 | 65 | 10-13 | 118 | 0.5 |
| | 2005/08/04 | 90 | 15-23 | 136 | 0.4 |
| HD 206860 | 2005/08/10 | 34 | $\gtrsim 13$[a] | 56 | 0.8 |
| | 2006/06/26 | 60 | $\gtrsim 15$[a] | 80 | 0.6 |
| HD 208313 | 2005/06/27 | 90 | 23-23 | 67 | 0.5 |
| | 2006/06/25 | 89 | 14-22 | 66 | 0.6 |
| V383 Lac | 2005/07/26 | 66 | 13-17 | 28 | 0.4 |
| | 2006/06/30 | 77 | 15-18 | 27 | 0.3 |
| HD 213845 | 2005/08/24 | 90 | - | 26 | 0.8 |
| | 2006/07/06 | 90 | - | 24 | 0.9 |
| GJ 875.1 | 2005/08/10 | 90 | 16-18 | 69 | 0.3 |
| | 2006/07/07 | 79 | 7-17 | 61 | 0.3 |
| GJ 876 | 2005/08/21 | 82 | 9-16 | 28 | 0.7 |
| GJ 9809 | 2005/08/04 | 90 | 18-20 | 25 | 0.3 |
| | 2006/09/14 | 120 | 25-27 | 31 | 0.3 |
| HD 220140 | 2005/08/05 | 90 | 16-18 | 21 | 0.6 |
| | 2006/07/16 | 82 | 7-9 | 19 | 0.7 |
| HD 221503 | 2005/08/31 | 90 | 21-22 | 28 | 0.5 |
| GJ 900 | 2004/08/24 | 90 | 15-21 | 17 | 0.5 |
| | 2005/09/08 | 90 | 16-22 | 46 | 0.4 |
| GJ 907.1 | 2005/09/07 | 65 | 5-15 | 22 | 0.4 |
| | 2006/07/17 | 44 | 8 | 16 | 0.4 |

[a]Only a lower estimate of the Strehl ratio can be obtained as the PSF peak is in the non-linear regime or sligthly saturated.

Table 3. Photometric uncertainties

| Sep. ($''$) | $< 4$ | $4 - 7$ | $7 - 10$ | $10 - 13$ | $> 13$ |
|---|---|---|---|---|---|
| $\sigma$ (mag) | 0.07 | 0.12 | 0.15 | 0.26 | 0.39 |

Table 4. GDPS detection limits[a]

| Name | 0.50″ | 0.75″ | 1.00″ | 1.25″ | 1.50″ | 2.00″ | 2.50″ | 3.00″ | 4.00″ | 5.00″ | 7.50″ | 10.00″ |
|---|---|---|---|---|---|---|---|---|---|---|---|---|
| HD 166 | - | - | 12.5 | 13.2 | 13.9 | 15.0 | 15.4 | 15.9 | 16.5 | 17.0 | 17.4 | 17.4 |
| HD 691 | 9.7 | 12.1 | 13.4 | 14.1 | 14.8 | 15.6 | 16.0 | 16.3 | 16.7 | 16.7 | 16.7 | 16.4 |
| HD 1405 | 9.3 | 11.4 | 12.8 | 13.5 | 14.0 | 14.8 | 15.3 | 15.7 | 16.1 | 16.2 | 16.2 | 15.9 |
| HD 5996 | - | 12.0 | 13.3 | 14.1 | 14.7 | 15.4 | 15.8 | 16.1 | 16.5 | 16.6 | 16.7 | 16.5 |
| HD 9540 | - | 11.9 | 13.2 | 14.0 | 14.7 | 15.5 | 16.0 | 16.5 | 17.1 | 17.3 | 17.6 | 17.5 |
| HD 10008 | - | 11.2 | 12.5 | 13.2 | 13.9 | 14.8 | 15.2 | 15.6 | 16.2 | 16.5 | 16.6 | 16.4 |
| GJ 82 | 9.0 | 10.5 | 11.8 | 12.6 | 13.2 | 13.8 | 14.3 | 14.6 | 14.9 | 15.0 | 14.8 | 14.6 |
| HD 14802 | - | - | - | 11.8 | 12.4 | 13.3 | 14.1 | 14.7 | 15.9 | 16.8 | 17.4 | 17.9 |
| HD 16765 | - | 11.1 | 13.0 | 14.0 | 14.6 | 15.4 | 15.8 | 16.3 | 16.9 | 17.4 | 17.6 | 17.6 |
| HD 17190 | - | 12.3 | 13.7 | 14.2 | 14.9 | 15.6 | 15.9 | 16.3 | 16.7 | 16.8 | 16.7 | 16.3 |
| HD 17382 | - | 12.1 | 13.3 | 14.1 | 14.7 | 15.5 | 15.9 | 16.3 | 16.8 | 17.0 | 17.0 | 16.7 |
| HD 17925 | - | 11.9 | 13.8 | 14.7 | 15.4 | 16.2 | 16.8 | 17.2 | 17.6 | 17.8 | 17.8 | 17.5 |
| HD 18803 | - | 11.3 | 12.9 | 13.8 | 14.6 | 15.6 | 16.1 | 16.5 | 16.8 | 17.1 | 17.2 | 17.0 |
| HD 19994 | - | 11.5 | 13.5 | 14.3 | 15.0 | 15.9 | 16.5 | 16.8 | 17.5 | 17.9 | 18.4 | 18.4 |
| HD 20367 | - | 10.0 | 11.7 | 12.3 | 12.9 | 13.9 | 14.5 | 14.9 | 15.6 | 16.1 | 16.4 | 16.2 |
| 2E 759 | 8.7 | 9.9 | 11.1 | 11.8 | 12.3 | 13.1 | 13.4 | 13.6 | 14.0 | 14.0 | 13.9 | 13.7 |
| HD 22049 | - | - | - | - | - | - | 16.0 | 16.5 | 17.3 | 17.7 | 18.6 | 19.0 |
| HIP 17695 | 10.0 | 11.8 | 12.9 | 13.6 | 14.3 | 14.8 | 15.2 | 15.4 | 15.7 | 15.8 | 15.7 | 15.4 |
| HD 25457 | - | - | 11.0 | 12.5 | 13.2 | 14.1 | 14.8 | 15.3 | 16.1 | 16.6 | 17.0 | 17.0 |
| HD 283750 | - | 12.2 | 13.5 | 14.3 | 15.1 | 16.0 | 16.4 | 16.9 | 17.2 | 17.3 | 17.1 | 16.8 |
| HD 30652 | - | - | - | - | - | 15.0 | 15.5 | 16.0 | 16.7 | 17.4 | 18.2 | 18.7 |
| GJ 182 | 10.0 | 11.9 | 13.2 | 14.0 | 14.7 | 15.4 | 15.8 | 16.1 | 16.5 | 16.6 | 16.5 | 16.2 |
| GJ 234A | 9.5 | 11.2 | 12.4 | 13.3 | 13.9 | 14.6 | 15.1 | 15.4 | 16.0 | 16.3 | 16.4 | 16.1 |
| GJ 281 | 7.7 | 10.4 | 12.1 | 12.9 | 13.5 | 14.4 | 14.7 | 15.1 | 15.3 | 15.4 | 15.4 | 15.2 |
| GJ 285 | 7.0 | 10.0 | 11.7 | 12.6 | 13.3 | 13.9 | 14.6 | 15.0 | 15.5 | 15.8 | 16.0 | 15.8 |
| HD 72905 | - | - | 11.3 | 12.5 | 13.1 | 14.3 | 15.0 | 15.4 | 16.3 | 16.8 | 17.4 | 17.7 |
| HD 75332 | - | 10.9 | 12.3 | 13.1 | 13.9 | 14.9 | 15.6 | 15.8 | 16.7 | 17.2 | 17.5 | 17.4 |
| HD 77407 | - | 10.3 | 11.4 | 12.3 | 13.1 | 14.1 | 14.8 | 15.1 | 15.7 | 16.0 | 16.4 | 16.2 |
| HD 78141 | - | 11.6 | 13.1 | 13.8 | 14.5 | 15.5 | 15.8 | 16.2 | 16.5 | 16.6 | 16.6 | 16.3 |
| HD 82558 | - | 11.5 | 12.9 | 13.8 | 14.5 | 15.5 | 15.9 | 16.2 | 16.7 | 16.9 | 17.0 | 16.8 |
| HD 82443 | - | 11.5 | 13.1 | 14.2 | 14.9 | 15.9 | 16.5 | 16.9 | 17.3 | 17.6 | 17.7 | 17.5 |
| GJ 393 | - | 11.9 | 13.3 | 14.1 | 14.8 | 15.6 | 16.1 | 16.3 | 16.7 | 16.9 | 17.0 | 16.8 |
| HD 90905 | - | 11.3 | 12.8 | 13.7 | 14.1 | 15.2 | 15.7 | 16.1 | 16.5 | 16.7 | 16.7 | 16.4 |
| HD 91901 | 7.7 | 10.1 | 11.5 | 12.2 | 12.8 | 13.7 | 14.1 | 14.4 | 14.9 | 14.9 | 14.9 | 14.7 |
| HD 92945 | - | 10.8 | 12.2 | 13.0 | 13.8 | 14.6 | 15.1 | 15.6 | 16.0 | 16.2 | 16.3 | 16.1 |
| HD 93528 | 8.5 | 10.2 | 11.7 | 12.6 | 13.3 | 14.3 | 14.8 | 15.0 | 15.5 | 15.7 | 15.9 | 15.7 |
| GJ 402 | 8.5 | 10.5 | 11.7 | 12.5 | 13.2 | 14.0 | 14.6 | 14.9 | 15.4 | 15.5 | 15.7 | 15.4 |
| HD 96064 | - | 12.3 | 13.5 | 14.3 | 15.0 | 15.6 | 16.1 | 16.3 | 16.6 | 16.9 | 16.9 | 16.7 |
| HD 97334 | - | 11.9 | 13.8 | 14.7 | 15.2 | 16.1 | 16.5 | 16.8 | 17.2 | 17.4 | 17.6 | 17.3 |
| HD 102195 | 9.8 | 12.2 | 13.3 | 14.2 | 14.8 | 15.5 | 16.0 | 16.2 | 16.5 | 16.6 | 16.6 | 16.4 |
| HD 102392 | 9.6 | 11.4 | 12.7 | 13.5 | 14.0 | 14.8 | 15.3 | 15.6 | 16.1 | 16.4 | 16.4 | 16.2 |
| HD 105631 | - | 11.7 | 12.9 | 13.6 | 14.2 | 15.1 | 15.6 | 16.1 | 16.5 | 16.8 | 16.8 | 16.6 |
| HD 107146 | - | 11.7 | 12.6 | 13.5 | 14.0 | 15.0 | 15.4 | 15.8 | 16.3 | 16.5 | 16.5 | 16.3 |
| HD 108767B | 8.6 | 10.6 | 12.0 | 12.8 | 13.5 | 14.4 | 14.9 | 15.2 | 15.7 | 15.9 | 16.0 | 15.7 |
| HD 109085 | - | - | - | 13.4 | 14.0 | 15.0 | 15.9 | 16.3 | 17.2 | 17.8 | 18.4 | 18.5 |
| BD+60 1417 | 10.2 | 12.0 | 13.1 | 13.8 | 14.2 | 14.8 | 15.1 | 15.3 | 15.6 | 15.5 | 15.5 | 15.2 |

Table 4—Continued

| Name | 0.50″ | 0.75″ | 1.00″ | 1.25″ | 1.50″ | 2.00″ | 2.50″ | 3.00″ | 4.00″ | 5.00″ | 7.50″ | 10.00″ |
|---|---|---|---|---|---|---|---|---|---|---|---|---|
| HD 111395 | - | - | 13.4 | 14.3 | 15.1 | 15.9 | 16.4 | 16.8 | 17.2 | 17.5 | 17.6 | 17.3 |
| HD 113449 | - | 11.6 | 12.7 | 13.7 | 14.0 | 15.0 | 15.5 | 15.8 | 16.3 | 16.5 | 16.6 | 16.4 |
| GJ 507.1 | 8.1 | 10.4 | 11.5 | 12.2 | 12.9 | 13.8 | 14.3 | 14.6 | 15.0 | 15.2 | 15.2 | 14.9 |
| HD 116956 | - | 11.4 | 12.8 | 13.6 | 14.3 | 15.1 | 15.7 | 16.1 | 16.5 | 16.7 | 16.9 | 16.7 |
| HD 118100 | 8.4 | 10.5 | 11.6 | 12.3 | 12.9 | 13.6 | 14.0 | 14.2 | 14.5 | 14.6 | 14.5 | 14.2 |
| GJ 524.1 | 10.2 | 12.0 | 13.1 | 13.7 | 14.3 | 14.9 | 15.2 | 15.4 | 15.5 | 15.6 | 15.4 | 15.1 |
| HD 124106 | - | 11.6 | 13.0 | 13.8 | 14.5 | 15.4 | 15.8 | 16.0 | 16.5 | 16.8 | 16.8 | 16.6 |
| HD 125161B | 10.6 | 12.4 | 13.6 | 14.4 | 14.7 | 15.4 | 15.8 | 16.0 | 16.3 | 16.5 | 16.4 | 16.1 |
| HD 129333 | 9.7 | 11.7 | 13.2 | 14.0 | 14.5 | 15.4 | 15.8 | 16.2 | 16.5 | 16.7 | 16.7 | 16.6 |
| HD 130004 | - | 12.1 | 13.3 | 14.1 | 14.6 | 15.4 | 15.8 | 16.1 | 16.5 | 16.8 | 16.7 | 16.4 |
| HD 130322 | 10.0 | 12.0 | 13.2 | 14.0 | 14.5 | 15.2 | 15.6 | 16.0 | 16.3 | 16.5 | 16.4 | 16.2 |
| HD 130948 | - | - | 12.4 | 13.3 | 13.9 | 14.8 | 15.4 | 15.7 | 16.5 | 16.9 | 17.4 | 17.3 |
| HD 135363 | 7.4 | 10.9 | 12.3 | 13.2 | 13.7 | 14.6 | 15.1 | 15.4 | 15.5 | 15.8 | 15.7 | 15.4 |
| HD 139813 | - | 10.3 | 11.4 | 12.0 | 12.7 | 13.7 | 14.4 | 15.0 | 15.8 | 16.2 | 16.3 | 16.2 |
| HD 141272 | - | 12.2 | 13.8 | 14.4 | 15.0 | 15.9 | 16.2 | 16.6 | 16.9 | 17.0 | 17.1 | 17.0 |
| HD 147379B | - | 11.3 | 12.9 | 13.6 | 14.1 | 15.0 | 15.3 | 15.6 | 15.9 | 16.0 | 16.0 | 15.8 |
| GJ 628 | - | 10.4 | 12.2 | 13.0 | 13.8 | 14.7 | 15.3 | 15.7 | 16.2 | 16.7 | 17.0 | 16.8 |
| HIP 81084 | 9.6 | 11.3 | 12.4 | 13.0 | 13.6 | 14.1 | 14.4 | 14.6 | 14.7 | 14.8 | 14.6 | 14.3 |
| HD 160934 | 9.5 | 11.1 | 12.6 | 13.3 | 13.9 | 14.6 | 14.9 | 15.0 | 15.3 | 15.3 | 15.2 | 14.9 |
| HD 162283 | 10.4 | 12.2 | 13.4 | 14.1 | 14.7 | 15.3 | 15.8 | 16.1 | 16.5 | 16.5 | 16.5 | 16.2 |
| HD 166181 | 9.3 | 11.7 | 13.0 | 13.7 | 14.4 | 15.1 | 15.5 | 15.9 | 16.3 | 16.5 | 16.6 | 16.3 |
| HD 167605 | 9.6 | 11.4 | 12.5 | 13.3 | 14.0 | 14.9 | 15.2 | 15.6 | 16.0 | 16.2 | 16.2 | 16.0 |
| HD 187748 | - | 11.8 | 13.0 | 13.8 | 14.5 | 15.4 | 15.9 | 16.3 | 17.0 | 17.4 | 17.6 | 17.4 |
| GJ 791.3 | 9.6 | 12.0 | 13.3 | 13.9 | 14.4 | 15.2 | 15.6 | 15.8 | 16.1 | 16.2 | 16.1 | 15.8 |
| HD 197481 | - | - | 11.1 | 11.7 | 12.5 | 13.5 | 14.3 | 14.8 | 15.6 | 16.2 | 16.4 | 16.4 |
| HD 201651 | 10.2 | 12.2 | 13.4 | 14.2 | 14.7 | 15.4 | 15.8 | 16.1 | 16.4 | 16.6 | 16.5 | 16.4 |
| HD 202575 | - | 11.3 | 12.6 | 13.4 | 14.1 | 15.0 | 15.6 | 16.1 | 16.6 | 16.8 | 17.0 | 16.8 |
| GJ 4199 | 10.6 | 12.0 | 13.2 | 13.8 | 14.5 | 15.2 | 15.6 | 15.7 | 16.0 | 16.1 | 15.9 | 15.5 |
| HD 206860 | - | 12.2 | 13.3 | 13.9 | 14.6 | 15.2 | 15.7 | 16.1 | 16.6 | 16.9 | 17.0 | 16.8 |
| HD 208313 | 10.9 | 13.0 | 14.1 | 14.8 | 15.3 | 16.1 | 16.5 | 16.8 | 17.2 | 17.3 | 17.3 | 17.1 |
| V383 Lac | 10.3 | 11.9 | 13.0 | 13.7 | 14.3 | 14.8 | 15.2 | 15.6 | 15.9 | 16.1 | 16.1 | 15.9 |
| HD 213845 | - | - | 13.3 | 14.0 | 14.8 | 15.7 | 16.3 | 16.8 | 17.2 | 17.7 | 18.1 | 18.1 |
| GJ 875.1 | 9.6 | 11.2 | 12.3 | 13.1 | 13.6 | 14.5 | 14.9 | 15.2 | 15.5 | 15.6 | 15.5 | 15.2 |
| GJ 876 | - | 10.1 | 11.1 | 12.2 | 12.7 | 13.8 | 14.4 | 15.1 | 15.8 | 16.2 | 16.6 | 16.6 |
| GJ 9809 | 11.2 | 12.9 | 14.1 | 14.6 | 15.1 | 15.6 | 15.9 | 16.0 | 16.3 | 16.4 | 16.2 | 15.9 |
| HD 220140 | - | 12.0 | 13.2 | 13.9 | 14.5 | 15.3 | 15.9 | 16.1 | 16.5 | 16.6 | 16.6 | 16.4 |
| HD 221503 | - | 11.8 | 13.2 | 14.0 | 14.6 | 15.4 | 15.9 | 16.3 | 16.7 | 17.0 | 17.2 | 17.0 |
| GJ 900 | 9.0 | 10.8 | 12.5 | 13.3 | 14.0 | 15.0 | 15.5 | 15.8 | 16.2 | 16.2 | 16.2 | 16.0 |
| GJ 907.1 | 8.5 | 9.9 | 11.2 | 12.1 | 12.6 | 13.4 | 14.0 | 14.3 | 14.9 | 15.1 | 15.2 | 15.0 |
| Median | 9.6 | 11.6 | 12.9 | 13.7 | 14.2 | 15.0 | 15.6 | 15.9 | 16.3 | 16.6 | 16.6 | 16.4 |
| Best | 11.2 | 13.0 | 14.1 | 14.8 | 15.4 | 16.2 | 16.8 | 17.2 | 17.6 | 17.9 | 18.6 | 19.0 |

[a]Magnitude difference in the NIRI CH4-short filter, at a $5\sigma$ level.

Table 5. Point sources detected

| Star | Epoch | Separation[a] (arcsec) | P.A.[b] (deg) | $\Delta m$[c] mag |
|---|---|---|---|---|
| HD 166 | 2005.6482 | 10.23 | 82.9 | 12.60 |
| HD 691 | 2005.6072 | 2.49 | 12.1 | 14.91 |
| HD 1405 | 2004.6409 | 3.95 | 254.0 | 13.98 |
| HD 5996 | 2005.6128 | 2.98 | 118.6 | 12.51 |
| | 2005.6128 | 4.78 | 71.6 | 13.23 |
| | 2005.6128 | 5.66 | 268.9 | 15.99 |
| | 2005.6128 | 6.95 | 73.9 | 15.43 |
| | 2005.6128 | 9.11 | 280.8 | 15.72[e] |
| | 2005.6128 | 9.15 | 228.1 | 15.67 |
| | 2005.6128 | 9.50 | 120.6 | 15.85[e] |
| | 2005.6128 | 9.58 | 205.2 | 13.51 |
| | 2005.6128 | 9.94 | 355.6 | 13.86 |
| | 2005.6128 | 10.33 | 221.6 | 10.86 |
| | 2005.6128 | 10.49 | 320.2 | 10.93 |
| | 2005.6128 | 10.55 | 296.5 | 14.41 |
| | 2005.6128 | 11.18 | 218.9 | 13.51 |
| | 2005.6128 | 13.09 | 215.7 | 14.63 |
| | 2005.6128 | 14.05 | 141.1 | 13.35 |
| | 2005.6128 | 14.57 | 314.9 | 11.48 |
| | 2005.6128 | 15.06 | 137.5 | 11.48 |
| HD 9540 | 2005.6182 | 5.51 | 308.8 | 14.63 |
| | 2005.6182 | 6.70 | 120.9 | 15.56 |
| GJ 82 | 2005.6647 | 4.24 | 78.2 | 13.89[d] |
| | 2005.6647 | 5.45 | 35.3 | 13.46[d] |
| | 2005.6647 | 6.27 | 157.0 | 11.06[d] |
| | 2005.6647 | 6.29 | 228.1 | 13.80[d] |
| | 2005.6647 | 6.42 | 307.0 | 13.08[d] |
| | 2005.6647 | 6.75 | 105.7 | 9.07[d] |
| | 2005.6647 | 6.83 | 106.4 | 9.23[d] |
| | 2005.6647 | 6.95 | 25.7 | 6.57[d] |

Table 5—Continued

| Star | Epoch | Separation[a] (arcsec) | P.A.[b] (deg) | $\Delta m$[c] mag |
|---|---|---|---|---|
| | 2005.6647 | 7.63 | 117.2 | 13.34[d] |
| | 2005.6647 | 8.82 | 315.9 | 9.27[d] |
| | 2005.6647 | 9.68 | 318.7 | 13.59[d] |
| | 2005.6647 | 9.74 | 334.0 | 13.11[d] |
| | 2005.6647 | 11.37 | 228.3 | 12.52[d] |
| HD 17382 | 2004.9740 | 11.78 | 130.8 | 13.16 |
| HD 18803 | 2004.9795 | 7.61 | 166.1 | 17.00 |
| | 2004.9795 | 7.98 | 208.3 | 15.68 |
| | 2004.9795 | 10.36 | 52.8 | 15.10 |
| HD 19994 | 2005.6648 | 6.18 | 187.4 | 17.62 |
| | 2005.6648 | 6.30 | 185.3 | 16.06 |
| | 2005.6648 | 11.64 | 72.7 | 17.51 |
| HD 283750 | 2004.8132 | 7.73 | 175.8 | 14.65 |
| | 2004.8132 | 12.72 | 104.2 | 13.85 |
| HD 30652 | 2005.6978 | 6.18 | 14.6 | 17.95[d] |
| | 2005.6978 | 9.53 | 241.4 | 18.33[d] |
| GJ 182 | 2004.8459 | 5.15 | 220.3 | 12.80 |
| | 2004.8459 | 7.44 | 233.7 | 10.61 |
| GJ 234A | 2005.8455 | 3.27 | 48.8 | 13.71[d] |
| | 2005.8455 | 6.64 | 304.9 | 16.01[d] |
| | 2005.8455 | 7.45 | 215.1 | 15.03[d] |
| | 2005.8455 | 10.08 | 179.3 | 13.36[d] |
| | 2005.8455 | 10.24 | 84.3 | 10.46[d] |
| | 2005.8455 | 11.75 | 103.0 | 12.58[d] |
| GJ 281 | 2005.2286 | 5.74 | 237.0 | 12.48 |
| | 2005.2286 | 8.80 | 288.4 | 12.92 |
| | 2006.1158 | 10.64 | 224.6 | 13.43[f] |
| GJ 285 | 2005.2095 | 8.83 | 114.3 | 11.55 |
| HD 75332 | 2005.3107 | 8.25 | 141.7 | 11.49 |
| HD 82443 | 2004.9829 | 5.27 | 190.3 | 11.64[d] |

Table 5—Continued

| Star | Epoch | Separation[a] (arcsec) | P.A.[b] (deg) | $\Delta m$[c] mag |
|---|---|---|---|---|
| | 2004.9829 | 5.42 | 191.5 | 16.65[d] |
| | 2004.9829 | 8.33 | 97.8 | 12.24[d] |
| | 2004.9829 | 10.17 | 164.8 | 16.14[d] |
| | 2004.9829 | 13.74 | 215.0 | 14.67[d] |
| HD 90905 | 2005.2098 | 5.47 | 188.2 | 10.91 |
| | 2005.2098 | 12.41 | 176.8 | 13.32 |
| HD 92945 | 2005.3983 | 9.77 | 236.2 | 12.82 |
| HD 93528 | 2005.3271 | 4.82 | 332.3 | 14.27[d] |
| GJ 402 | 2006.1273 | 12.46 | 324.0 | 10.80[f] |
| | 2005.3164 | 13.88 | 337.7 | 10.10 |
| HD 96064 | 2005.2972 | 4.69 | 29.7 | 15.99[e] |
| | 2005.2972 | 5.94 | 213.8 | 8.18 |
| | 2005.2972 | 6.11 | 213.6 | 10.76 |
| | 2005.2972 | 8.90 | 329.7 | 15.90 |
| HD 102195 | 2005.3109 | 11.94 | 185.5 | 13.82 |
| HD 102392 | 2005.3082 | 5.72 | 42.0 | 15.02 |
| | 2005.3082 | 10.57 | 308.9 | 14.99[e] |
| HD 108767B | 2005.3055 | 6.72 | 87.7 | 12.41 |
| | 2005.3055 | 8.28 | 100.1 | 14.62 |
| | 2005.3055 | 10.20 | 123.9 | 15.10 |
| HD 109085 | 2005.3986 | 12.92 | 256.2 | 15.80 |
| BD+60 1417 | 2005.2946 | 2.05 | 298.4 | 8.76 |
| | 2005.2946 | 14.08 | 133.5 | 12.80[e] |
| HD 116956 | 2005.4067 | 9.34 | 17.4 | 15.05 |
| GJ 524.1 | 2005.2948 | 7.59 | 19.7 | 13.09 |
| HD 124106 | 2005.2975 | 7.51 | 124.8 | 13.85 |
| | 2005.2975 | 9.39 | 342.2 | 9.51 |
| | 2005.2975 | 9.60 | 341.1 | 8.71 |
| | 2005.2975 | 10.39 | 287.5 | 14.65 |
| | 2005.2975 | 11.17 | 291.7 | 14.18 |

Table 5—Continued

| Star | Epoch | Separation[a] (arcsec) | P.A.[b] (deg) | $\Delta m$[c] mag |
|---|---|---|---|---|
| | 2005.2975 | 12.06 | 120.6 | 15.45 |
| HD 130322 | 2005.4014 | 7.61 | 329.8 | 11.00 |
| HD 130948 | 2005.2922 | 2.60 | 103.1 | 8.56[g] |
| | 2005.2922 | 2.66 | 104.0 | 8.83[g] |
| HD 135363 | 2005.2949 | 7.50 | 122.1 | 10.28 |
| HD 139813 | 2005.4097 | 6.85 | 271.3 | 14.48[d] |
| | 2005.4097 | 7.36 | 272.2 | 14.79[d] |
| HD 141272 | 2005.2977 | 2.31 | 12.3 | 11.44 |
| | 2005.2977 | 4.03 | 286.9 | 16.59[e] |
| | 2005.2977 | 8.04 | 305.4 | 15.78[e] |
| | 2005.2977 | 8.32 | 258.1 | 15.66 |
| | 2005.2977 | 10.95 | 299.2 | 9.90 |
| | 2005.2977 | 11.43 | 190.4 | 15.14 |
| | 2005.2977 | 12.26 | 209.5 | 12.31 |
| GJ 628 | 2005.2924 | 5.19 | 259.0 | 16.32[e] |
| | 2005.2924 | 6.29 | 161.6 | 14.81 |
| | 2005.2924 | 10.25 | 232.1 | 14.90 |
| | 2005.2924 | 10.52 | 2.8 | 13.42[e] |
| | 2005.2924 | 11.49 | 308.6 | 14.88 |
| | 2005.2924 | 12.72 | 228.6 | 15.10 |
| | 2005.2924 | 13.64 | 215.4 | 15.03 |
| HIP 81084 | 2005.2979 | 6.84 | 234.6 | 13.10 |
| | 2005.2979 | 8.64 | 4.5 | 13.70 |
| | 2005.2979 | 9.69 | 49.6 | 11.22 |
| | 2005.2979 | 9.98 | 68.4 | 13.04 |
| | 2005.2979 | 14.04 | 226.4 | 11.60 |
| HD 160934 | 2005.2952 | 4.08 | 319.2 | 11.03 |
| | 2005.2952 | 8.94 | 232.9 | 9.96 |
| HD 162283 | 2005.3007 | 2.76 | 118.7 | 15.54 |
| | 2005.3007 | 3.41 | 154.4 | 14.13 |

Table 5—Continued

| Star | Epoch | Separation[a] (arcsec) | P.A.[b] (deg) | $\Delta m$[c] mag |
|---|---|---|---|---|
| | 2005.3007 | 3.26 | 4.9 | 15.21 |
| | 2005.3007 | 3.68 | 244.8 | 14.01 |
| | 2005.3007 | 3.94 | 152.8 | 14.22 |
| | 2005.3007 | 4.22 | 158.8 | 12.52 |
| | 2005.3007 | 4.47 | 111.9 | 15.21 |
| | 2005.3007 | 4.37 | 23.1 | 13.23 |
| | 2005.3007 | 4.70 | 299.8 | 15.44 |
| | 2005.3007 | 4.95 | 80.0 | 10.82 |
| | 2005.3007 | 5.24 | 124.0 | 16.08 |
| | 2005.3007 | 5.24 | 191.8 | 13.38 |
| | 2005.3007 | 5.23 | 348.9 | 15.59 |
| | 2005.3007 | 6.07 | 72.2 | 14.49 |
| | 2005.3007 | 6.61 | 159.4 | 12.06 |
| | 2005.3007 | 6.72 | 84.6 | 14.28 |
| | 2005.3007 | 6.89 | 352.8 | 13.50 |
| | 2005.3007 | 7.11 | 91.2 | 8.65 |
| | 2005.3007 | 7.38 | 176.6 | 16.29 |
| | 2006.7069 | 7.42 | 18.0 | 15.95[f] |
| | 2005.3007 | 7.33 | 78.7 | 15.73 |
| | 2005.3007 | 7.47 | 75.0 | 12.53 |
| | 2005.3007 | 7.71 | 134.8 | 12.62 |
| | 2005.3007 | 7.94 | 110.5 | 15.55 |
| | 2005.3007 | 8.19 | 198.2 | 15.44 |
| | 2005.3007 | 8.37 | 173.6 | 15.88 |
| | 2005.3007 | 8.60 | 243.7 | 14.96 |
| | 2005.3007 | 8.69 | 132.5 | 15.01 |
| | 2006.7069 | 9.01 | 318.9 | 15.97[f] |
| | 2005.3007 | 9.08 | 141.2 | 12.99 |
| | 2005.3007 | 9.23 | 152.7 | 15.98 |
| | 2005.3007 | 9.32 | 142.4 | 14.95 |

Table 5—Continued

| Star | Epoch | Separation[a] (arcsec) | P.A.[b] (deg) | $\Delta m$[c] mag |
|---|---|---|---|---|
| | 2005.3007 | 9.37 | 205.7 | 13.88 |
| | 2005.3007 | 9.28 | 337.0 | 12.77 |
| | 2005.3007 | 9.63 | 235.2 | 15.38 |
| | 2005.3007 | 9.56 | 78.8 | 13.78 |
| | 2006.7069 | 9.86 | 286.6 | 15.74[f] |
| | 2006.7069 | 10.03 | 289.1 | 15.75[f] |
| | 2005.3007 | 10.20 | 97.7 | 13.31 |
| | 2005.3007 | 10.18 | 37.3 | 8.81 |
| | 2005.3007 | 10.31 | 319.4 | 14.47 |
| | 2005.3007 | 10.48 | 308.7 | 15.38 |
| | 2005.3007 | 10.71 | 337.2 | 14.52 |
| | 2005.3007 | 10.92 | 36.3 | 11.98[e] |
| | 2005.3007 | 11.36 | 249.0 | 13.24 |
| | 2005.3007 | 11.38 | 112.7 | 9.04 |
| | 2005.3007 | 11.80 | 40.1 | 14.79[e] |
| | 2006.7069 | 12.00 | 261.7 | 15.23[f] |
| | 2005.3007 | 12.01 | 329.6 | 9.78 |
| | 2005.3007 | 12.28 | 153.9 | 14.26 |
| | 2006.7069 | 12.28 | 265.3 | 13.99[f] |
| | 2005.3007 | 12.43 | 114.8 | 9.89[e] |
| | 2006.7069 | 12.47 | 71.5 | 14.76[f] |
| | 2005.3007 | 12.40 | 100.7 | 13.16 |
| | 2005.3007 | 12.61 | 111.8 | 13.37[e] |
| | 2005.3007 | 13.04 | 16.9 | 14.10[e] |
| | 2006.7069 | 13.21 | 161.5 | 13.02[f] |
| | 2006.7069 | 13.46 | 65.5 | 14.51[f] |
| | 2005.3007 | 13.53 | 303.6 | 12.68[e] |
| | 2006.7069 | 13.59 | 257.1 | 11.76[f] |
| | 2005.3007 | 14.12 | 314.4 | 12.55[e] |
| | 2005.3007 | 14.59 | 112.9 | 10.20[e] |

Table 5—Continued

| Star | Epoch | Separation[a] (arcsec) | P.A.[b] (deg) | $\Delta m$[c] mag |
|---|---|---|---|---|
| | 2005.3007 | 14.66 | 17.4 | 12.43[e] |
| | 2005.3007 | 14.74 | 34.6 | 11.81[e] |
| HD 166181 | 2005.2925 | 10.38 | 53.4 | 14.40 |
| | 2005.2925 | 11.21 | 195.8 | 15.04 |
| | 2005.2925 | 13.40 | 167.6 | 14.19[e] |
| | 2005.2925 | 14.46 | 262.8 | 11.93[e] |
| HD 187748 | 2005.3965 | 5.51 | 325.9 | 15.76 |
| | 2005.3965 | 7.93 | 277.1 | 13.01 |
| | 2005.3965 | 8.02 | 276.7 | 12.18 |
| | 2005.3965 | 12.81 | 114.3 | 9.74 |
| | 2005.3965 | 13.15 | 321.5 | 12.52 |
| | 2006.7043 | 15.02 | 311.3 | 14.90[f] |
| GJ 791.3 | 2005.3992 | 1.98 | 341.2 | 12.03[d] |
| | 2005.3992 | 2.39 | 51.3 | 13.51[d] |
| | 2005.3992 | 3.77 | 289.0 | 10.92[d] |
| | 2005.3992 | 3.80 | 137.6 | 13.99[d] |
| | 2005.3992 | 3.87 | 19.4 | 10.01[d] |
| | 2005.3992 | 4.38 | 201.6 | 14.31[d] |
| | 2005.3992 | 5.55 | 300.0 | 12.72[d] |
| | 2005.3992 | 5.96 | 49.6 | 10.28[d] |
| | 2005.3992 | 6.56 | 232.8 | 12.91[d] |
| | 2005.3992 | 6.66 | 155.9 | 13.37[d] |
| | 2005.3992 | 6.73 | 254.7 | 12.93[d] |
| | 2005.3992 | 8.01 | 10.3 | 13.03[d] |
| | 2005.3992 | 8.25 | 143.8 | 15.03[d] |
| | 2005.3992 | 8.31 | 71.5 | 15.02[d] |
| | 2005.3992 | 8.36 | 155.7 | 13.62[d] |
| | 2005.3992 | 8.89 | 177.3 | 12.86[d] |
| | 2005.3992 | 9.33 | 10.5 | 14.93[d] |
| | 2005.3992 | 9.55 | 276.2 | 15.45[d] |

Table 5—Continued

| Star | Epoch | Separation[a] (arcsec) | P.A.[b] (deg) | $\Delta m$[c] mag |
|---|---|---|---|---|
| | 2005.3992 | 9.64 | 195.5 | 14.14[d] |
| | 2005.3992 | 9.89 | 347.0 | 15.16[d] |
| | 2005.3992 | 10.05 | 255.1 | 14.63[d] |
| | 2005.3992 | 10.12 | 201.2 | 13.28[d] |
| | 2005.3992 | 10.21 | 310.6 | 14.36[d] |
| | 2005.3992 | 10.22 | 328.8 | 10.56[d] |
| | 2005.3992 | 10.55 | 166.9 | 15.14[d] |
| | 2005.3992 | 10.63 | 80.3 | 13.51[d] |
| | 2005.3992 | 10.75 | 326.6 | 11.48[d] |
| | 2005.3992 | 10.80 | 57.8 | 10.86[d] |
| | 2005.3992 | 10.84 | 51.7 | 14.67[d] |
| | 2005.3992 | 11.26 | 243.5 | 9.22[d] |
| | 2005.3992 | 11.58 | 315.9 | 9.96[d] |
| | 2005.3992 | 11.71 | 14.8 | 13.26[d] |
| | 2005.3992 | 12.17 | 18.6 | 11.27[d] |
| | 2005.3992 | 12.45 | 46.6 | 12.52[d] |
| | 2005.3992 | 12.80 | 274.4 | 11.86[d] |
| | 2005.3992 | 13.07 | 127.8 | 11.44[d] |
| | 2005.3992 | 13.08 | 75.4 | 13.58[d] |
| | 2005.3992 | 13.23 | 81.0 | 11.26[d] |
| | 2005.3992 | 13.73 | 70.5 | 8.91[d] |
| | 2005.3992 | 14.41 | 65.8 | 11.04[d] |
| | 2005.3992 | 15.14 | 356.5 | 11.98[d] |
| | 2005.3992 | 15.23 | 179.8 | 12.02[d] |
| HD 201651 | 2005.4867 | 3.67 | 201.4 | 12.48 |
| | 2005.4867 | 8.39 | 259.1 | 12.90 |
| | 2005.4867 | 14.53 | 331.5 | 13.75[e] |
| HD 202575 | 2005.5386 | 5.54 | 28.5 | 12.41 |
| | 2005.5386 | 12.37 | 168.0 | 13.98 |
| GJ 4199 | 2004.6431 | 9.16 | 319.9 | 12.24 |

Table 5—Continued

| Star | Epoch | Separation[a] (arcsec) | P.A.[b] (deg) | $\Delta m$[c] mag |
|---|---|---|---|---|
| | 2004.6431 | 11.76 | 177.6 | 10.58 |
| HD 206860 | 2005.6069 | 3.67 | 60.0 | 15.13 |
| HD 208313 | 2005.4868 | 2.93 | 30.6 | 14.78 |
| | 2005.4868 | 6.24 | 31.1 | 9.69 |
| | 2005.4868 | 9.45 | 301.0 | 14.41 |
| | 2005.4868 | 10.45 | 137.8 | 16.50[e] |
| | 2005.4868 | 11.43 | 151.6 | 15.85 |
| | 2005.4868 | 13.23 | 121.0 | 13.73 |
| | 2005.4868 | 13.51 | 33.2 | 14.61 |
| | 2005.4868 | 15.13 | 63.8 | 12.00 |
| V383 Lac | 2005.5660 | 4.00 | 100.0 | 14.14 |
| | 2005.5660 | 4.02 | 79.3 | 15.98 |
| | 2005.5660 | 4.63 | 204.6 | 11.81 |
| | 2005.5660 | 4.70 | 207.7 | 14.89 |
| | 2005.5660 | 8.49 | 181.6 | 14.82 |
| | 2005.5660 | 9.09 | 110.0 | 11.65 |
| | 2005.5660 | 9.55 | 358.6 | 14.15 |
| | 2005.5660 | 10.59 | 93.0 | 8.48 |
| | 2005.5660 | 11.68 | 142.3 | 11.24 |
| HD 213845 | 2005.6453 | 12.85 | 214.2 | 14.91 |
| GJ 875.1 | 2005.6071 | 7.83 | 343.9 | 9.40 |
| | 2005.6071 | 8.97 | 260.7 | 12.73 |
| | 2005.6071 | 11.42 | 151.3 | 12.30 |
| | 2005.6071 | 14.54 | 15.2 | 11.85[e] |
| GJ 9809 | 2006.7019 | 2.10 | 240.4 | 15.30[f] |
| | 2005.5907 | 2.18 | 30.6 | 12.91 |
| | 2006.7019 | 3.22 | 141.6 | 15.55[f] |
| | 2005.5907 | 3.35 | 207.8 | 12.31 |
| | 2005.5907 | 3.55 | 337.2 | 11.53 |
| | 2005.5907 | 3.79 | 173.8 | 11.92 |

Table 5—Continued

| Star | Epoch | Separation[a] (arcsec) | P.A.[b] (deg) | $\Delta m$[c] mag |
|---|---|---|---|---|
| | 2006.7019 | 4.51 | 0.9 | 16.23[f] |
| | 2005.5907 | 5.37 | 258.1 | 14.38 |
| | 2006.7019 | 5.66 | 118.3 | 15.35[f] |
| | 2005.5907 | 6.39 | 68.9 | 15.47 |
| | 2005.5907 | 7.01 | 101.1 | 9.69 |
| | 2005.5907 | 7.34 | 236.9 | 13.49 |
| | 2005.5907 | 7.69 | 127.3 | 11.26 |
| | 2005.5907 | 7.75 | 131.1 | 14.21 |
| | 2006.7019 | 7.92 | 78.4 | 15.65[f] |
| | 2006.7019 | 9.08 | 247.3 | 14.84[f] |
| | 2005.5907 | 9.18 | 36.5 | 15.03 |
| | 2005.5907 | 9.23 | 27.2 | 14.80 |
| | 2005.5907 | 9.51 | 95.2 | 12.35 |
| | 2006.7019 | 9.58 | 84.1 | 15.30[f] |
| | 2005.5907 | 9.98 | 68.5 | 14.35 |
| | 2005.5907 | 9.98 | 121.4 | 10.42 |
| | 2006.7019 | 10.02 | 163.4 | 15.37[f] |
| | 2005.5907 | 10.18 | 93.9 | 13.69 |
| | 2006.7019 | 10.73 | 12.2 | 15.33[f] |
| | 2005.5907 | 10.64 | 248.1 | 13.59 |
| | 2005.5907 | 10.94 | 254.4 | 9.90 |
| | 2005.5907 | 11.23 | 82.9 | 13.75 |
| | 2006.7019 | 11.40 | 336.1 | 15.18[f] |
| | 2005.5907 | 11.69 | 155.9 | 12.14 |
| | 2005.5907 | 11.87 | 32.2 | 12.28 |
| | 2005.5907 | 11.74 | 291.2 | 7.01 |
| | 2005.5907 | 12.23 | 310.2 | 8.73 |
| | 2005.5907 | 12.75 | 66.9 | 12.76 |
| | 2005.5907 | 13.03 | 58.0 | 11.09 |
| | 2005.5907 | 12.93 | 332.5 | 13.42 |

Table 5—Continued

| Star | Epoch | Separation[a] (arcsec) | P.A.[b] (deg) | $\Delta m$[c] mag |
|---|---|---|---|---|
| | 2005.5907 | 14.04 | 309.7 | 12.50 |
| HD 220140 | 2005.5934 | 6.14 | 358.5 | 15.96 |
| | 2005.5934 | 15.19 | 50.4 | 10.62[e] |
| HD 221503 | 2005.6646 | 9.02 | 234.4 | 15.61[d] |
| GJ 900 | 2004.6458 | 7.41 | 76.0 | 14.20 |
| | 2004.6458 | 12.15 | 150.6 | 12.53 |
| | 2004.6458 | 12.41 | 96.4 | 9.36 |
| GJ 907.1 | 2005.6837 | 7.93 | 296.7 | 13.68 |

Note. — Target stars around which no point source was detected are omitted from this table. Unless stated otherwise, all point sources listed were confirmed to be background objects using data from two epochs.

[a]Uncertainty is 0.015″, see text for detail.

[b]Uncertainty is 0.2°, see text for detail.

[c]Uncertainties are given in Table 3, see text for detail.

[d]No second epoch data available.

[e]Source undetected in second epoch data.

[f]Source detected in second epoch data only.

[g]Previously known brown dwarf companion (Potter et al. 2002; Goto et al. 2002).

Table 6. Properties of newly resolved binary systems

| Star | Epoch | Separation (″) | P.A. (°) | Brightness ratio[a] |
|---|---|---|---|---|
| HD 14802 | 2005.6348 | $0.469 \pm 0.005$ | $267.1 \pm 0.7$ | $12 \pm 2$ |
| HD 135363 | 2005.2950 | $0.302 \pm 0.002$ | $129.9 \pm 0.5$ | $4.0 \pm 0.1$ |
| | 2006.1277 | $0.316 \pm 0.002$ | $131.8 \pm 0.5$ | |
| HD 160934 | 2005.2953 | $0.213 \pm 0.002$ | $268.5 \pm 0.7$ | $2.2 \pm 0.1$ |
| | 2006.7097 | $0.218 \pm 0.002$ | $271.3 \pm 0.7$ | |
| HD 166181 | 2005.2926 | $0.065 \pm 0.005$ | $16.2 \pm 5.0$ | $5.5 \pm 0.4$ |
| | 2006.7124 | $0.102 \pm 0.003$ | $51.5 \pm 2.0$ | |
| HD 213845 | 2005.6453 | $6.09 \pm 0.03$ | $129.8 \pm 0.4$ | –[b] |
| | 2006.5108 | $6.09 \pm 0.03$ | $129.6 \pm 0.4$ | |

[a]Brightness of the primary over that of the companion.

[b]The peak of both the primary and companion are saturated in the data.

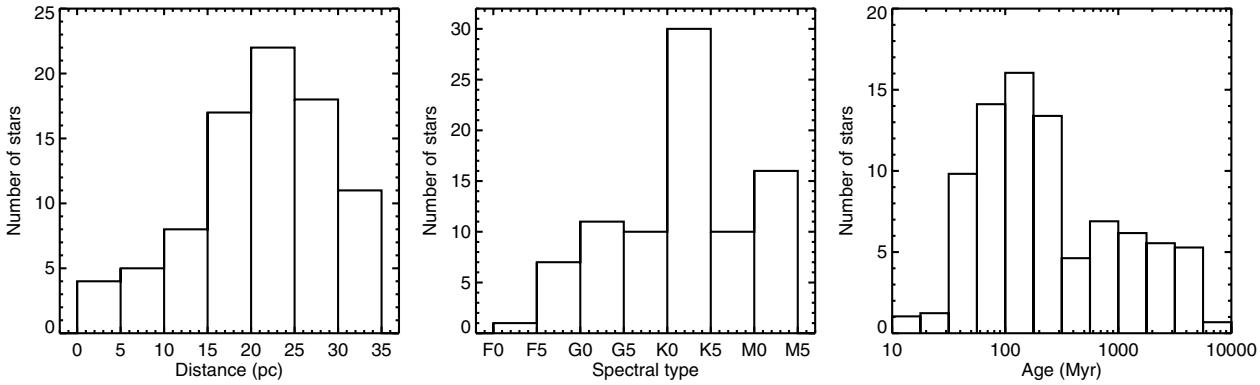


Fig. 1.— Distribution of distance, spectral type, and age of the target stars. For the age distribution, each star was distributed over all the age bins according to the fraction of their estimated age interval falling inside each bin.

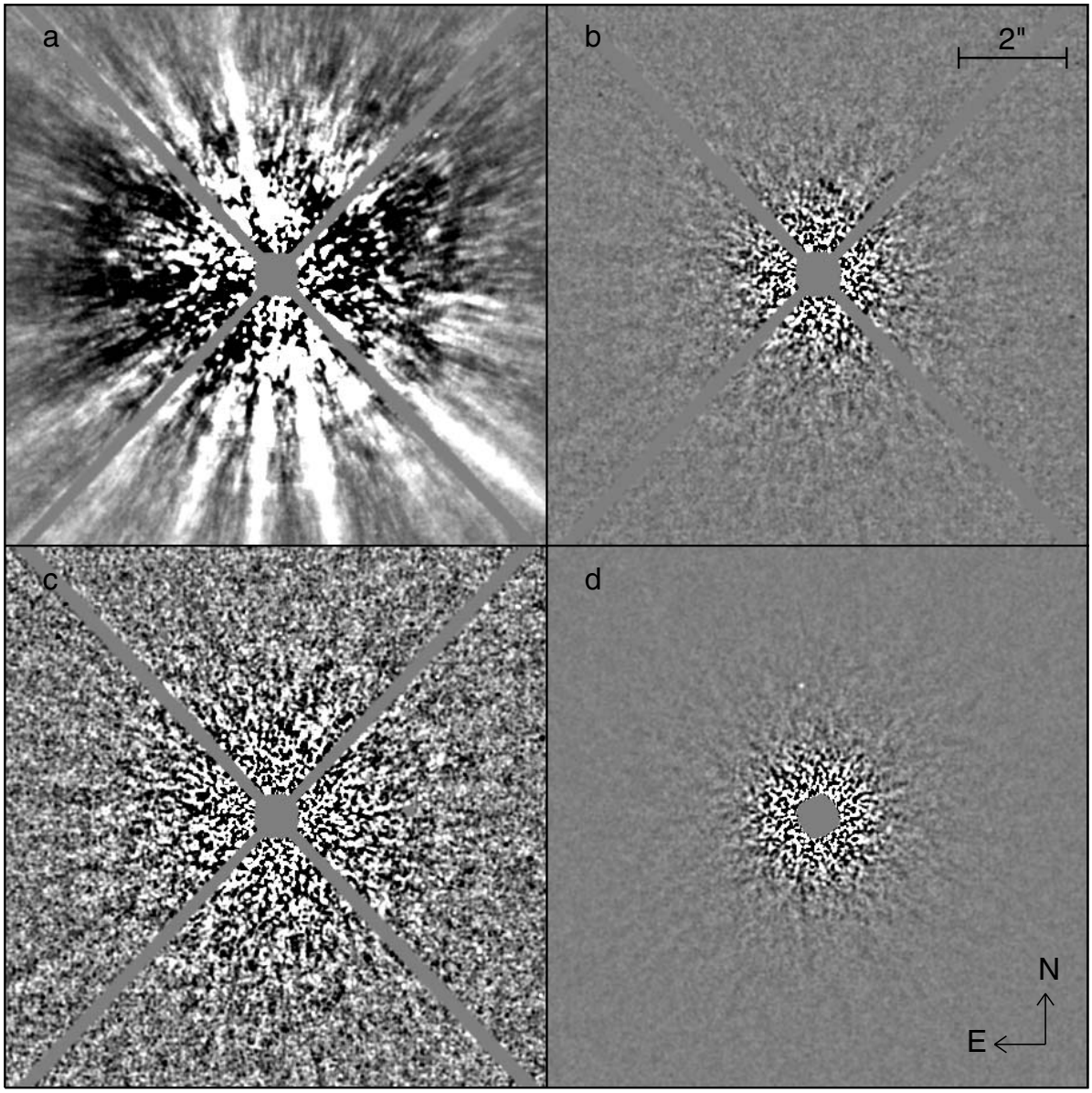


Fig. 2.— Illustration of the ADI noise attenuation process. Panel (a) shows an original 30-s image of the young star HD 691 after subtraction of an azimuthally symmetric median intensity profile, panels (b) and (c) both show, with a different intensity scale, the corresponding residual image after ADI subtraction, and panel (d) shows the median combination of 117 such residual images. Display intensity ranges are $\pm 5 \times 10^{-6}$ and $\pm 10^{-6}$ of stellar PSF peak for the top and bottom rows respectively. Each panel is $10''$ on a side. The diffraction spikes from the secondary mirror support vanes and the central saturated region are masked. The faint point source ($\Delta m = 14.9$) visible in panel (d) at a separation of $2.43''$ and P.A. of $7.3^\circ$ could not have been detected without ADI processing.

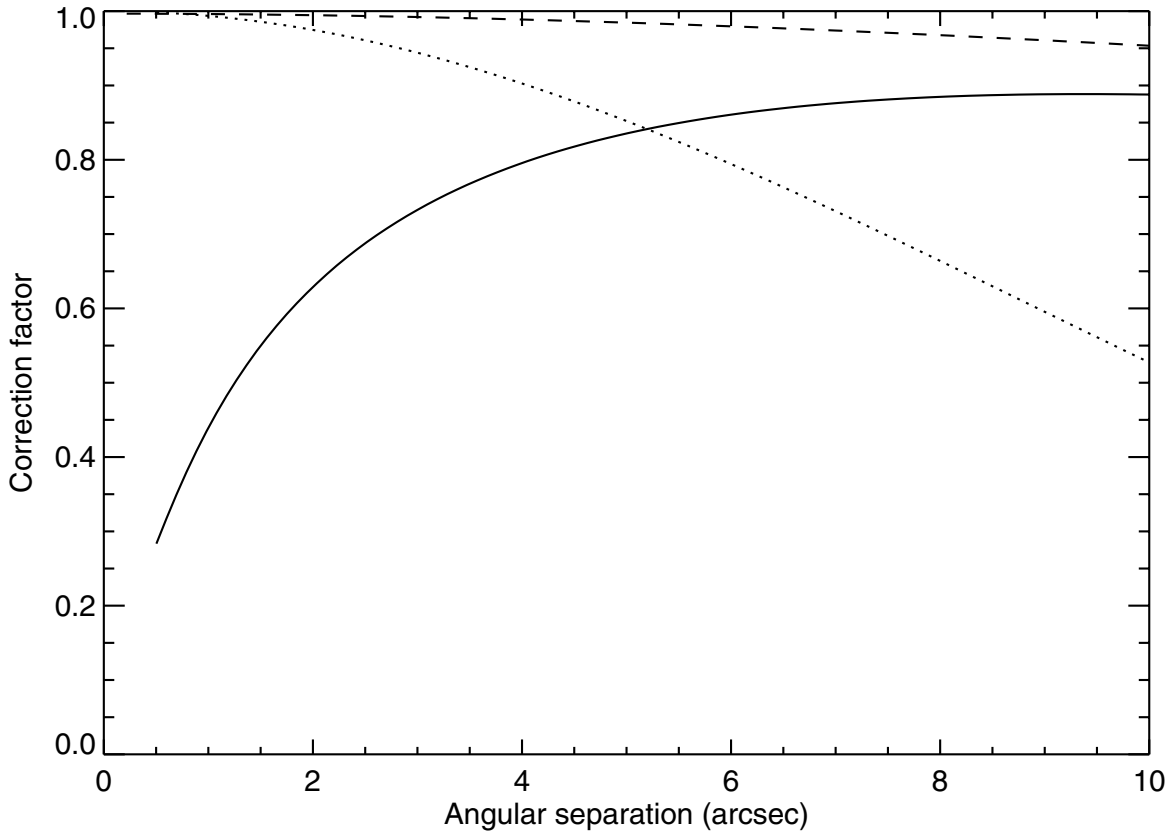


Fig. 3.— Typical values of $f_{\rm sub}$ (*solid line*), $f_{\rm aniso}$ (*dotted line*), and $f_{\rm sm}$ (*dashed line*) as a function of angular separation.

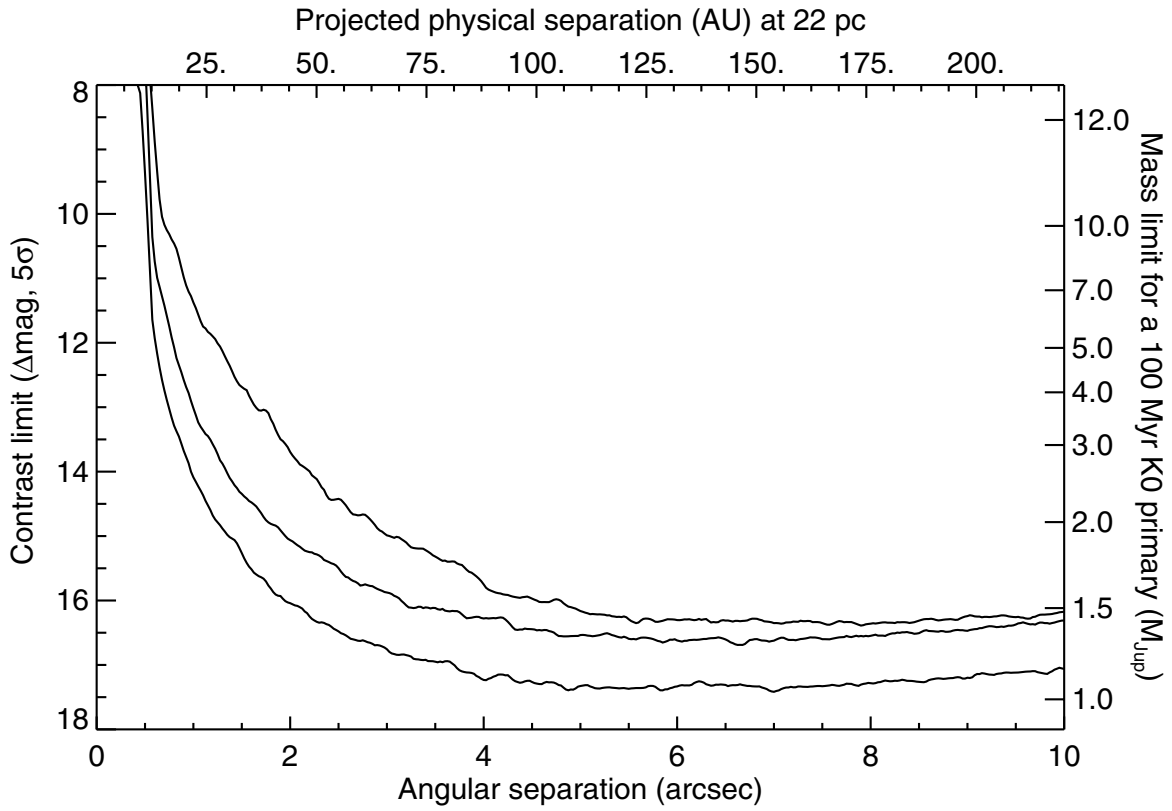


Fig. 4.— Survey detection limits in difference of magnitude (in the NIRI CH4-short filter) between an off-axis point source and the target star, at the $5\sigma$ level. The top, middle, and bottom curves are representative of, respectively, poor, median, and good performance reached by the survey.

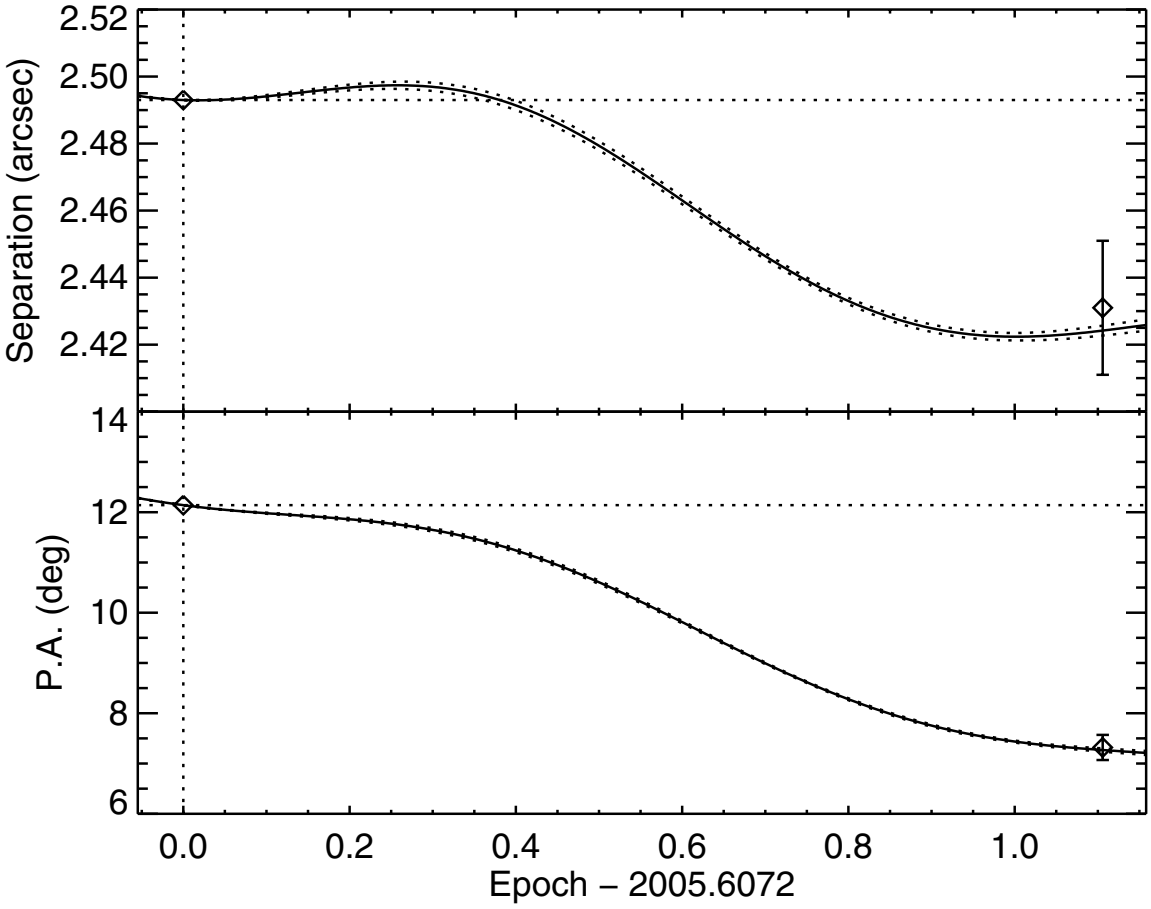


Fig. 5.— Verification of the physical association of the point source detected around the young star HD 691. Open diamonds mark the observed separation (*top*) and P.A. (*bottom*) of the point source at the two epochs. The solid line indicates the expected separation and P.A. of a distant background source as a function of time. The observations agree very well with the expected motion of a background source, indicating that the source is not associated with HD 691.

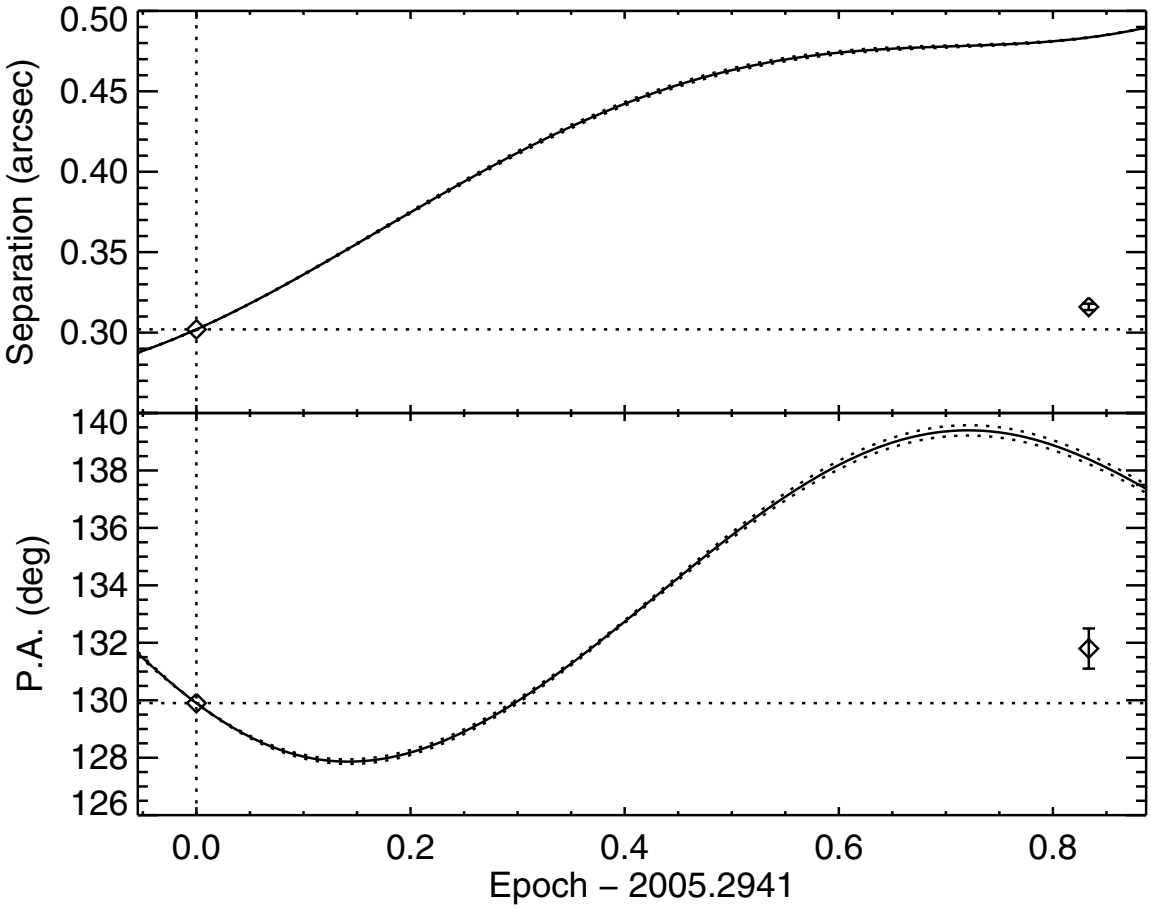


Fig. 6.— Verification of the physical association of the point source detected around HD 135363. Open diamonds mark the observed separation (*top*) and P.A. (*bottom*) of the point source at the two epochs. The solid line indicates the expected separation and P.A. of a distant background source as a function of time.

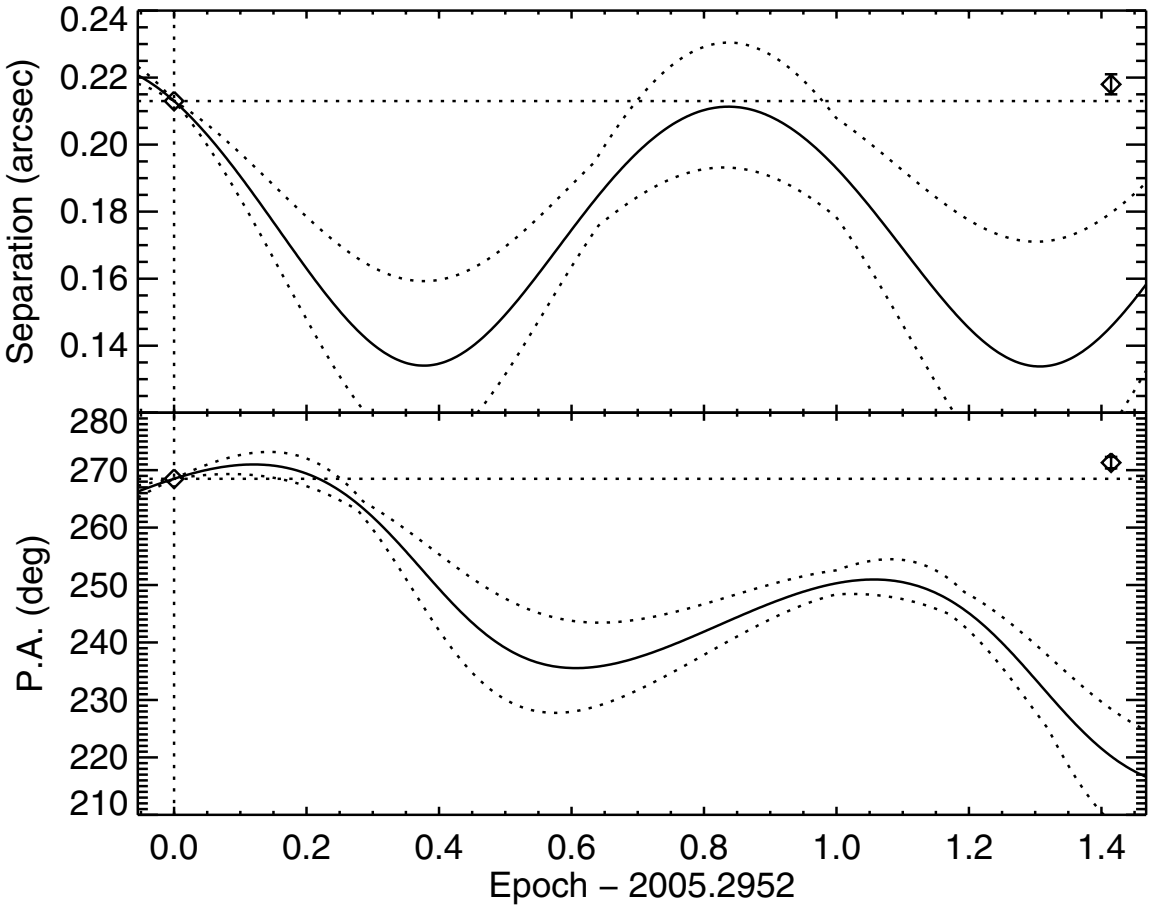


Fig. 7.— Same as Figure 6 for HD 160934.

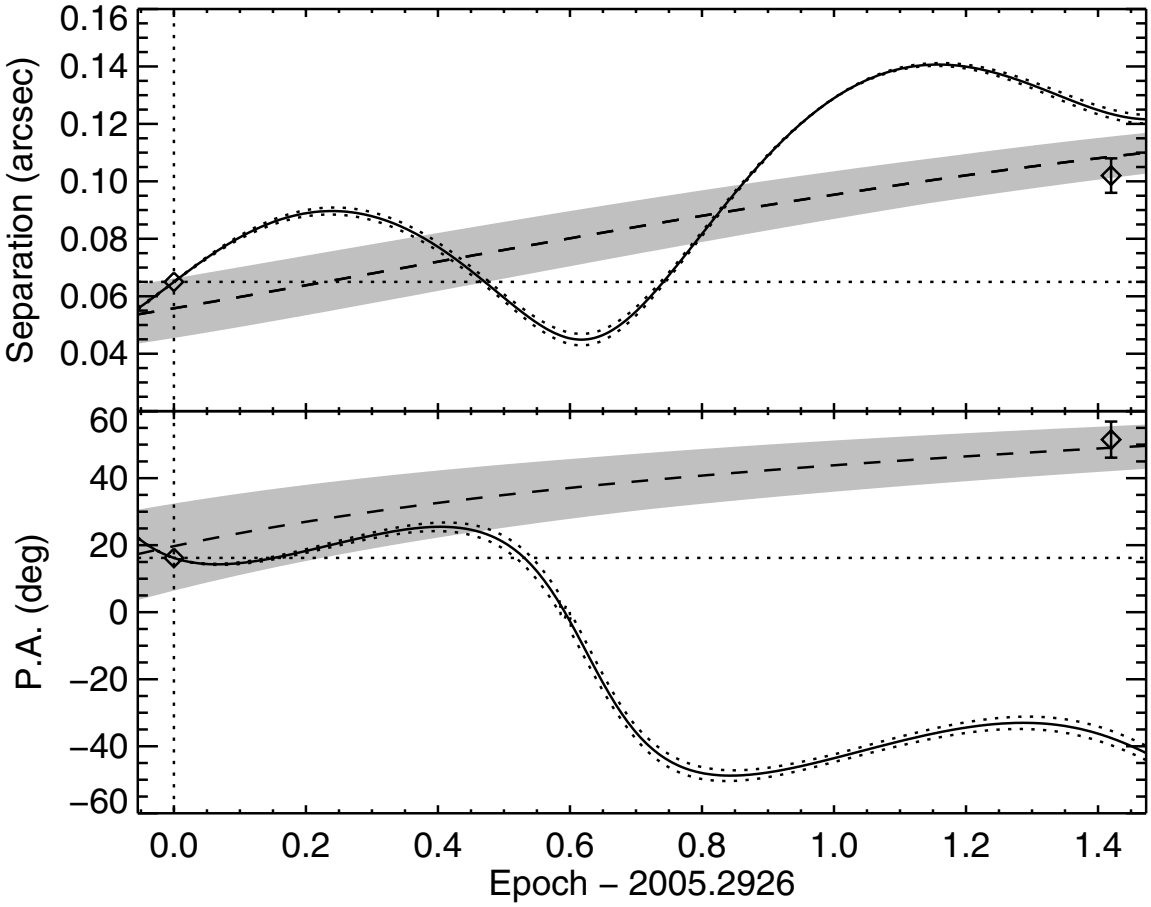


Fig. 8.— Same as Figure 6 for HD 166181. The predicted separation and P.A. of HD 166181B based on the astrometric solution of Fekel et al. (2005) are shown as *dashed lines*, with uncertainties indicated by the shaded areas.

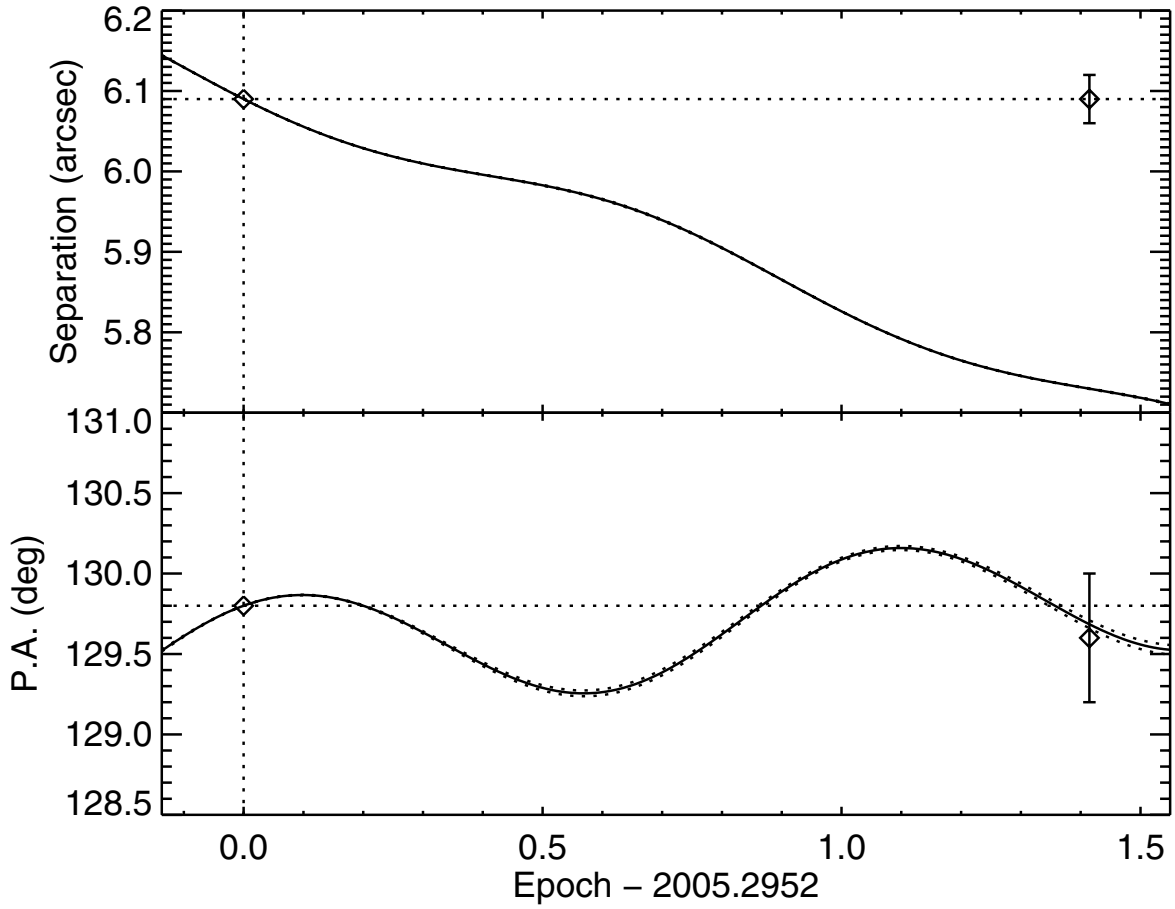


Fig. 9.— Same as Figure 6 for HD 213845

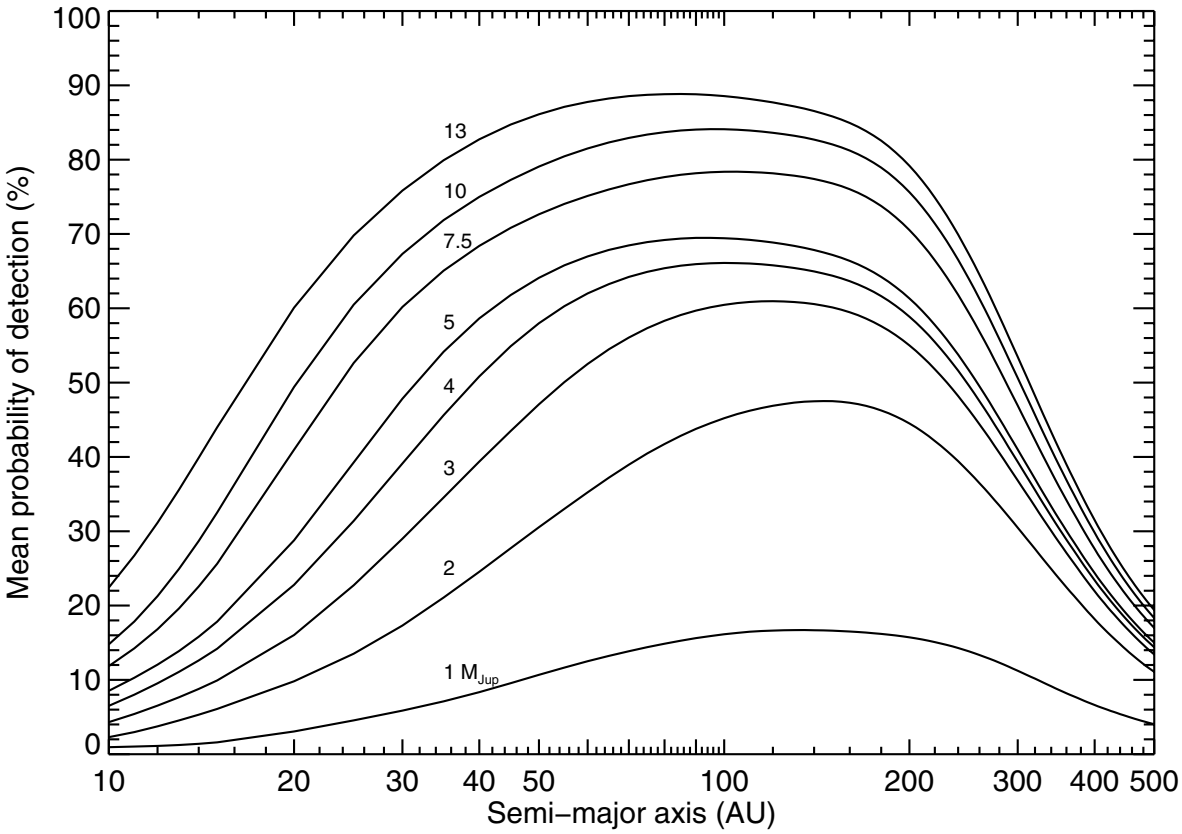


Fig. 10.— Mean probability of detection of a planet of given mass as a function of the semi-major axis of its orbit; the curves are labeled by the mass of the planet, in $M_{\rm Jup}$. The mean is obtained over all targets of the survey.

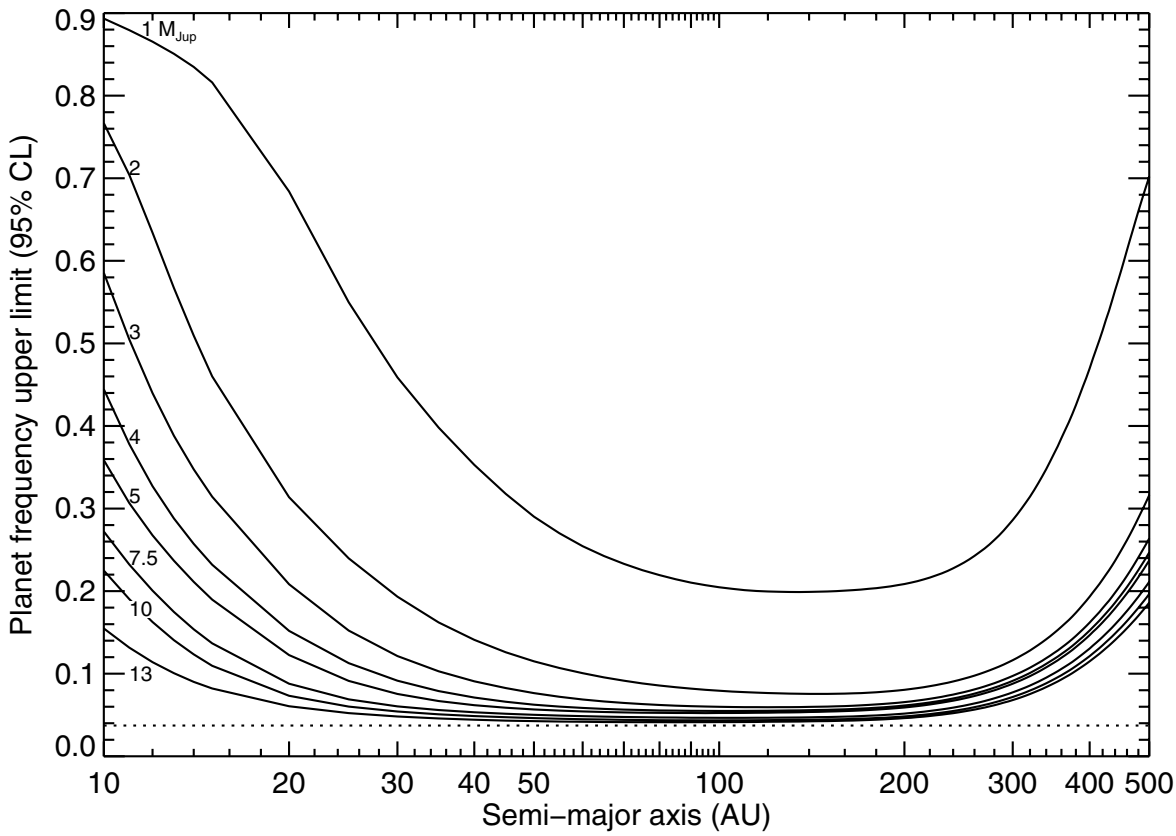


Fig. 11.— Upper limits, at the 95% CL, on the fraction of stars harboring at least one companion of mass in the range $[m_{\rm min}, 40]$ $M_{\rm Jup}$ and orbit of semi-major axis in various ranges. The minimum mass, $m_{\rm min}$, is indicated on each curve. For any interval, $[a_{\rm min}, a_{\rm max}]$ AU, of semi-major axis selected, the correct value of $f_{\rm max}$ to read from the graph is the maximum of the curve within that interval. The curves shown in this graph are conservative upper limits that are valid for any distributions of mass and semi-major axis. The dotted line indicates the minimum upper limit that one could derive from observation of 79 stars if the probability of detection of a planet was 100% irrespective of its age, mass, and orbital separation.

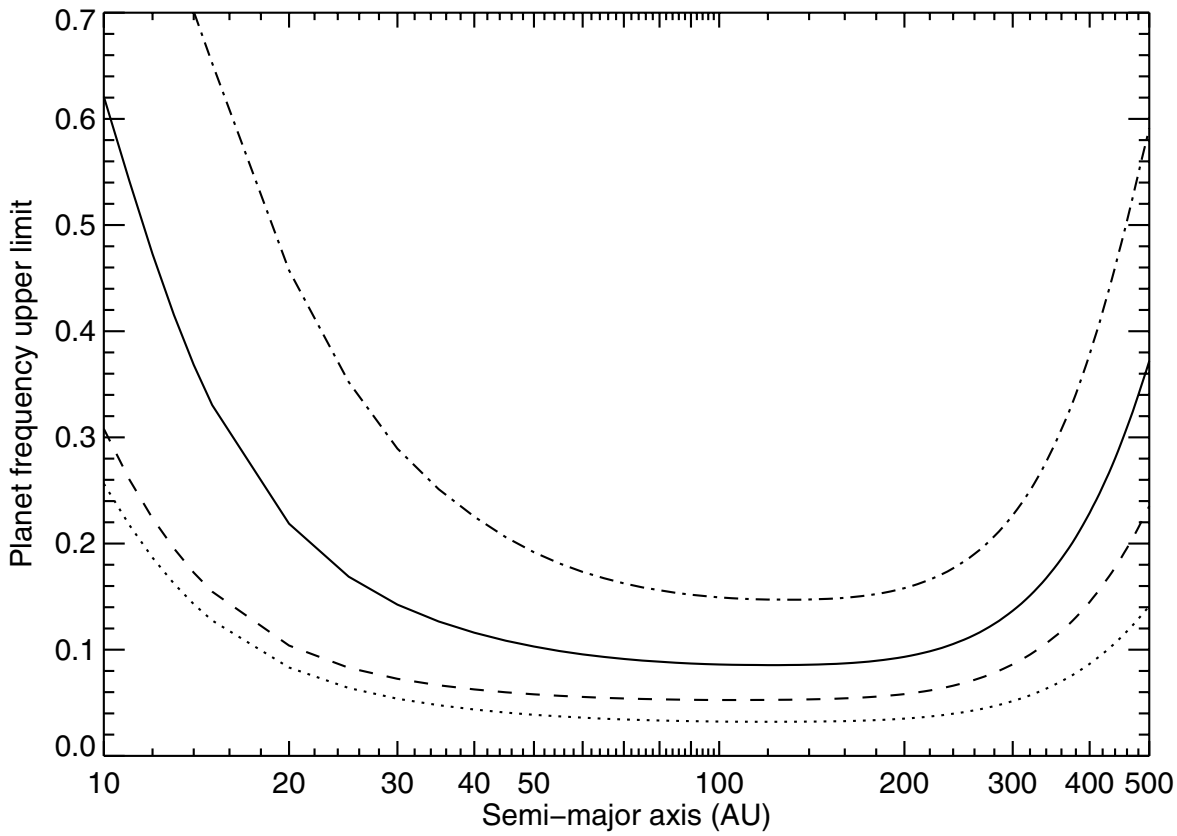


Fig. 12.— Upper limits, at the 95% CL, on the fraction of stars harboring at least one planet of mass in the range $[0.5, 13]$ $M_{\rm Jup}$, assuming $\mathrm{d}n/\mathrm{d}m \propto m^{\beta}$, and semi-major axis in various ranges. The values of $\beta$ are $-2$ (*dot-dashed line*), $-1.2$ (*solid line*), and 0 (*dashed line*). For any interval, $[a_{\rm min}, a_{\rm max}]$ AU, of semi-major axis selected, the correct value of $f_{\rm max}$ to read from the graph is the maximum of the curve within that interval. The 67% CL curve for $\beta = -1.2$ is also shown (*dotted line*).

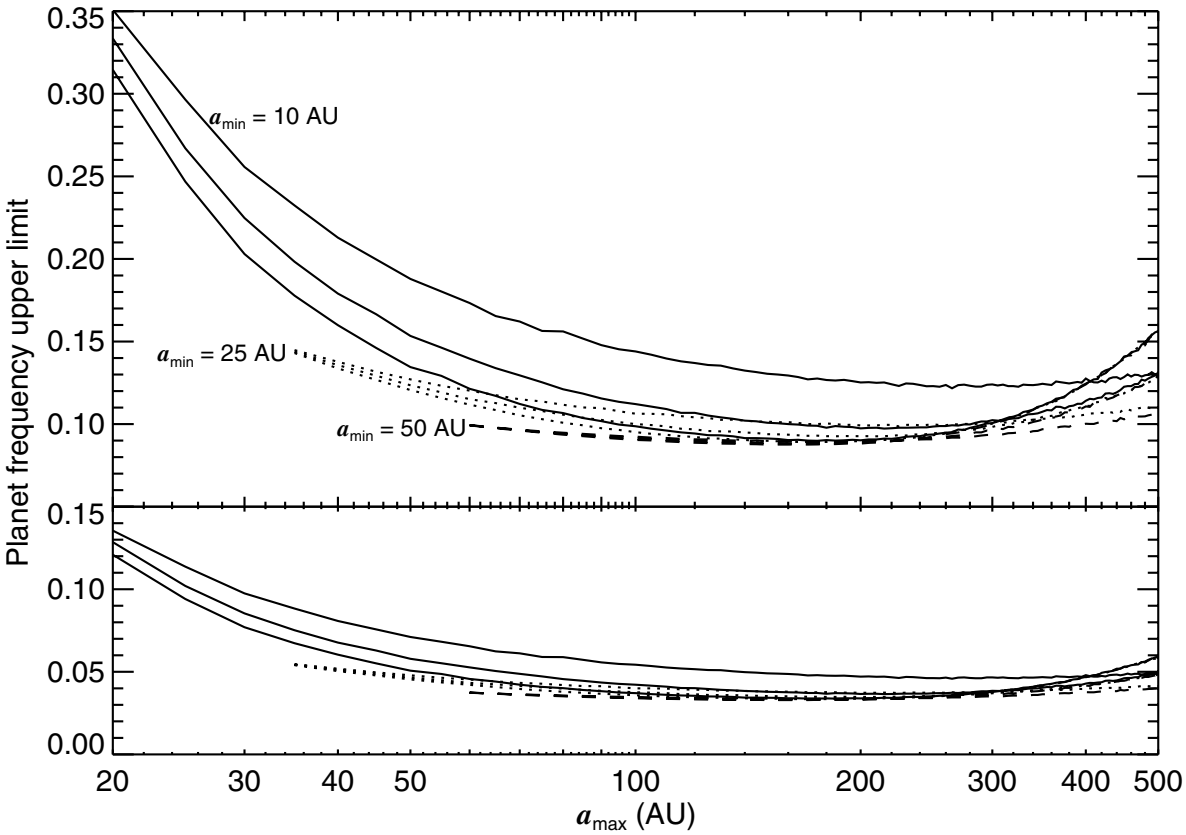


Fig. 13.— Upper limit, at the 95% CL (*top panel*) or 67% CL (*bottom panel*), on the fraction of stars harboring at least one giant planet of mass in the range $[0.5, 13]$ $M_{\rm Jup}$, assuming $\mathrm{d}n/\mathrm{d}m \propto m^{-1.2}$, and orbit of semi-major axis in the range $[a_{\rm min}, a_{\rm max}]$ AU, assuming $\mathrm{d}n/\mathrm{d}a \propto a^{\gamma}$. The abcissa indicates the upper bounds ($a_{\rm max}$) of the semi-major axis intervals, while the lower bounds ($a_{\rm min}$) are 10 AU (*solid lines*), 25 AU (*dotted lines*), and 50 AU (*dashed lines*). The top, middle, and bottom curves in each set of three curves are for $\gamma = -1$, 0, and 1, respectively.